Texas A&M University
Mechanical Engineering Department
Turbomachinery Laboratory
Tribology Group

Thermohydrodynamic Analysis of Bump Type Gas Foil Bearings: Model and Predictions

Research Progress Report to the TAMU Turbomachinery Research Consortium

TRC-B&C-2-08

by

Luis San Andrés

Mast-Childs Professor

Principal Investigator

Tae Ho Kim

Post-Doctoral Research Associate

June 2008

This material is based upon work supported by NASA Research Announcement NNH06ZEA001N-SSRW2, Fundamental Aeronautics: Subsonic Rotary Wing Project 2

Prediction of Foil Bearing Performance: A Computational Model Anchored to Test Data
Texas Engineering Experiment Station Project # 32525/39600/ME
TRC Project TEES# 32513/1519C4

EXECUTIVE SUMMARY

Thermohydrodynamic Analysis of Bump Type Gas Foil Bearings: Model and Predictions

TRC-B&C-2-08

Ready use of gas foil bearings (GFBs) into high temperature applications requires accurate model prediction accounting for transport and disposal of thermal energy. Adequate thermal management is a pervasive performance problem and engineering design challenge in micro gas turbines, for example. The current research introduces a thermohydrodynamic (THD) model for mechanical energy dissipation and thermal energy transport by the thin gas film and cooling gas streams (inner or outer), as well as heat conduction into the bearing cartridge. A bulk-flow model describes the transport of momentum and thermal energy within the gas film. Equivalent heat transfer coefficients represent multilayer convection/conduction paths. The model also accounts for shaft thermal expansion and centrifugal growth due to increases in rotor temperature and rotor speed. Material properties of the underlying foil structure degrade as the temperature increases.

THD model predictions show a larger minimum film thickness (and smaller journal eccentricity) when compared to those for the isothermal flow model, in particular with large static loads, because increases in gas film temperature result in net increases in gas viscosity. Larger shaft temperatures mean larger gas film temperatures with shaft thermal expansion reducing the operating bearing clearance, and leading to increases in drag torque. As the shaft temperature increases, the journal eccentricity and the minimum film thickness decrease due to the reduction in the operating bearing clearance. A cooling flow stream on the back of the top foil increases the heat flow transport to reduce the film temperature.

Note from Editor: TRC-B&C-2-08 reproduces Quarter 1 Progress Report to NASA (Nov. 2007). Current report edited four times prior to its release to TRC members.

TABLE OF CONTENTS

LIST OF TABLES

LIST OF FIGURES

NOMENCLATURE

c	Thin film radial clearance, a function of temperature [m]
c_p	Gas specific heat at constant pressure [I/kg-K]
D	Diameter [m], D=2 R
e_X, e_Y	Journal eccentricity components [m], $e = \sqrt{e_X^2 + e_Y^2}$
E	Young's modulus [N/ m^2]
h	film thickness [m]
H_b	Bump height [m]
$\bar{h}$	Heat convection coefficient [W/m^2-K]
k_B	(simple) Bump foil stiffness/unit area [(N/m)/m^2]
L	Bearing axial width [m]
l_B	Half bump arc length [m]
l_x	Pad circumferential length, $R(\Theta_t - \Theta_l)$ [m]
Nu	*Nusselt* number
N_b, N_s	Number of bumps, Number of bump strips
P	Gas pressure [Pa]
R	Radius [m]
$\Re_g$	Ideal gas constant [J/kg-K]
r_p	Preload [m]
S_C, S_T	Centrifugal growth and thermal expansion [m]
T	Bulk Temperature [°C]
t	Time [s]
t_b	Bump thickness [m]
t_t	Top (thin) foil thickness [m]
U, W	Bulk-flow gas velocities in circumferential (x) and axial (z) direction
U_m	Mean circumferential flow velocity [m/s]
w_d	top foil transverse deflection [m]
X, Y, Z	Inertial Cartesian coordinate system [m]
$x = R\,\Theta, z$	Coordinate system on plane of bearing [m]
α_T	Thermal expansion coefficient [-]
α_Ω	Inlet pre-swirl factor for circumferential velocity [-]
κ	Thermal conductivity [W/m-K]
ρ	Gas density [kg/m^3]
λ	Thermal inlet mixing ratio [-]
μ	Gas viscosity [Pa-s]
ν	Poisson's ratio [-]
$\wp_r$	*Prandtl* number, $\wp_r = \dfrac{c_p\,\mu}{\kappa}$
Θ	Circumferential coordinate [rad]
Ω, ω	Rotor angular velocity and whirl frequency [rad]

Subscripts

cooling	Cooling gas flow
l,t,p	Leading and trailing edge of top foil, and offset position
f	Thin gas film
i, o	Inner and outer
O	Outer flow region
S	Shaft (journal)
supply	Fresh gas (natural) supply at the leading edge of top foil
B	Bearing
F	Foil
a	Ambient

INTRODUCTION

The widespread usage of foil gas bearing (GFB) into oil-free turbomachinery relies on overcoming intermittent contact and damaging wear at start up and shut down, temporary rubs during normal operating conditions; and most importantly, engineering thermal management to ensure reliable GFB performance in high temperature environments. Although, gains have been made in specific loading [1-2], high-temperature material limits, coating endurance and stability, and adequate thermal management still restrict application of GFBs into high power density gas turbines.

Advancements in GFBs toward their reliable operation in high temperature environments require of accurate performance prediction that accounts for thermal effects. The report details the extension of the existing GFB computational model – isothermal & isoviscous ideal gas, see Refs. [3-4], to include the thermal energy transport within the thin gas film region, heat convection from/into the thin film into/from the rotating shaft and the top foil, and heat conduction through the bump strip layer and into/from the bearing housing.

Model predictions follow for a generation I GFB with axial length L and diameter D of 38.1 mm which supports a shaft with an increasing temperature from 25 °C (room temperature) to 150 °C (moderately high temperature), which simulates a engine shaft with heat conducted from a hot turbine, for example. Model predictions also reveal the effect of an adequate cooling mechanism (proven thermal management [5]) to carry away heat conducted from hot components or generated due to the mechanical power dissipated within the gas film.

LITERATURE REVIEW

The archival literature shows a few references that include modeling of heat flow transport in gas bearings. Salehi et al. [6] implemented a simple *Couette* flow approximation to predict the temperature field evolving around the bearing circumference. Comparison of exit temperature predictions to measurements conducted on a test GFB are in reasonable agreement. Most important, however, is the finding that about 80% of the thermal energy is conducted by the top foil and advected to a cooling stream forced axially at one end of the bearing.

Peng and Khonsari [7] introduce a more comprehensive thermohydrodynamic (THD) model to predict the steady-state performance of GFBs. A simple elastic foundation represents the foil structure with coupled Reynolds and thermal energy transport equations solved simultaneously

for prediction of the gas film pressure and temperature fields. No shaft centrifugal growth and thermal expansion are accounted for. The outer cooling flow regime determines appropriate heat convection coefficients. Predictions reveal a nearly uniform film temperature along the bearing axial direction; and with an increase in load capacity since typical gas viscosity increases with temperature. Comparison of predicted temperatures to test data given in Ref. [6] is noted as excellent. However, Radil and Zeszotek [8] find a decrease of ~30 % in load capacity for a GFB tested at increasing temperatures ranging from 25ºC to 650 ºC. Apparently, temperature dependent mechanical properties of the structural components and actual dimensions (thermal growth) need be accounted for reliable predictions.

Le Lez [9] implements a bulk flow model to predict the gas film pressure and temperature fields within GFBs. The top foil and the bump strip layer are modeled as a nonlinear elastic foundation with dry friction between the top foil and the bearing housing. Analysis of the thermohydrodynamic model uses an upwind scheme to solve the energy transport equation, which accounts for heat convection/conduction to the shaft and bearing housing. Predicted gas film peak temperatures increase as the journal eccentricity (load) increases. The THD model predicts a larger load capacity than an isothermal flow model with the same operating conditions.

Feng and Kaneko [10] predict the gas film pressure and temperature fields within multiwound foil bearings. A FE model of the Reynolds and energy transport equations provides the gas film pressure and temperature fields. Model predictions show that the THD model predicts larger load capacity and drag torque than the isothermal flow model. The gas film peak temperature increases as the static load increases and as the rotor speed increases. A comparison of model predictions to test data, obtained for a bump type GFB tested in Ref. [6], shows reasonable agreement.

Sim and Kim [11] predict 3D gas film temperature fields within a flexure pivot tilting pad gas bearing using Reynolds equation and energy transport equation. The model accounts for heat flux from the gas film to the shaft/bearing housing and the shaft thermal expansion and centrifugal growth. Predictions show that the gas film temperature increases as the rotor speed increases. The film temperature hardly changes with increasing static loads and for different numbers of tilting pads. The THD model predicts larger direct stiffness and damping coefficients than the isothermal flow model, in particular at high rotor speeds, due to an increase in the gas viscosity and a decrease in the bearing actual clearance.

Thermal seizure and failure of a GFB are the result of inadequate thermal management and poor design with little consideration to the whole rotor-bearing system – thermal and structural. A micro-turbine manufacturer [12] using proprietary GFB technology downplays the importance of thermal effects and notes that engineered energy conduction paths in the bearing cartridge are paramount to the success of their product application. Hence, the implementation of a realistic thermal model for GFBs must include not only the mechanical energy dissipation occurring within the gas film, but most importantly the heat convection and conduction paths into and out of the bounding surfaces (shaft and bearing) with due attention to the structural-thermal coupling that changes the GFB structural properties, sizes of components (shaft diameter and operating *minimum film* thickness).

THERMODYNAMIC ANALYSIS OF GAS FOIL BEARINGS

DESCRIPTION OF THERMAL ENERGY TRANSPORT MODEL

A comprehensive thermohydrodynamic (THD) model for thermal energy transport in a gas foil bearing-rotor system does not include just the thin film gas region but also the cooling streams, inner and/or outer, typically found in existing rotor-GFBs systems, as well as the conduction through the bearing shell and in the rotating shaft. Figure 1 (a) shows the schematic view of a bump-type foil bearing supporting a rotating hollow shaft. The graph depicts the coordinate systems and major components of the GFB. For generality, two cooling gas flow streams are supplied as noted. Figure 1 (b) illustrates a cross-sectional view of the GFB with the cooling streams, inner and outer. For purposes of the discussion below, consider – as in a gas turbine – the shaft is at a high temperature T_S due to a heat conducted from a hot section. The two cooling streams are:

(a) **Inner flow stream,** at supply temperature and pressure $\left(T_{C_i}, P_{C_i}\right)$ flowing through the hollow shaft to cool directly the shaft inner surface at temperature T_{S_i} ; and/or

(b) **Outer flow stream,** at supply temperature and pressure $\left(T_{C_o}, P_{C_o}\right)$ flowing axially through one end of the FB structure to cool directly the back face of the top foil at temperature T_{Fo}. Along the bearing axial coordinate $\left(0 \le z \le L\right)$, the outer stream temperature (T_O) increases

as it removes heat, while its pressure (P_O) decreases to ambient condition (P_a).

Importantly enough, there is also pressurized gas flowing axially through the **thin film region** separating the rotating shaft from the topfoil front face. In this region, the gas hydrodynamic film pressure (P_f) is generated while its temperature (T_f) varies. The outer stream $\left(T_{C_o}, P_{C_o}\right)$ also sets the inlet or entrance conditions into the thin gas film. Note that the inner gas film is characterized by a minute film thickness (h_f), while the outer flow underneath the top foil has a larger gap with characteristic length equal to a bump foil height (Δ_B).

Within the thin gas film, mechanical power generated by fluid drag and heat convected from the *hot* shaft is removed[1] by the inner film gas flow and also conducted through the top foil at temperature T_F. The outer cooling stream, at temperature T_O increasing axially, advects part of the conducted heat; while the remnant heat flows through conduction into the bearing housing at temperature $T_{B,}$ and disposed into an external fluid medium at temperature T_∞.

In practice, however, one or the other cooling methods will be implemented. It would not be efficient to implement both methods at once.

[1] This assertion implies the gas film is at a lower temperature than the shaft outer surface. The opposite case, i.e. where thermal energy flows from the film into the shaft, requires the shaft to be at a lower temperature and an inner cooling stream. Note that a solid shaft (journal) becomes a source or sink of thermal energy for the cases described above, respectively.

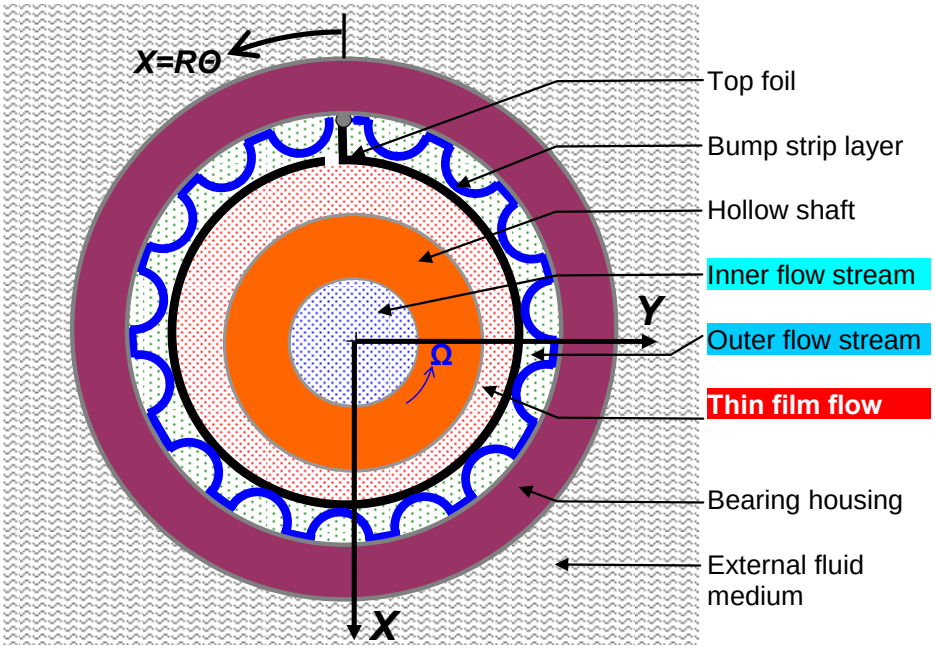

(a) Front view

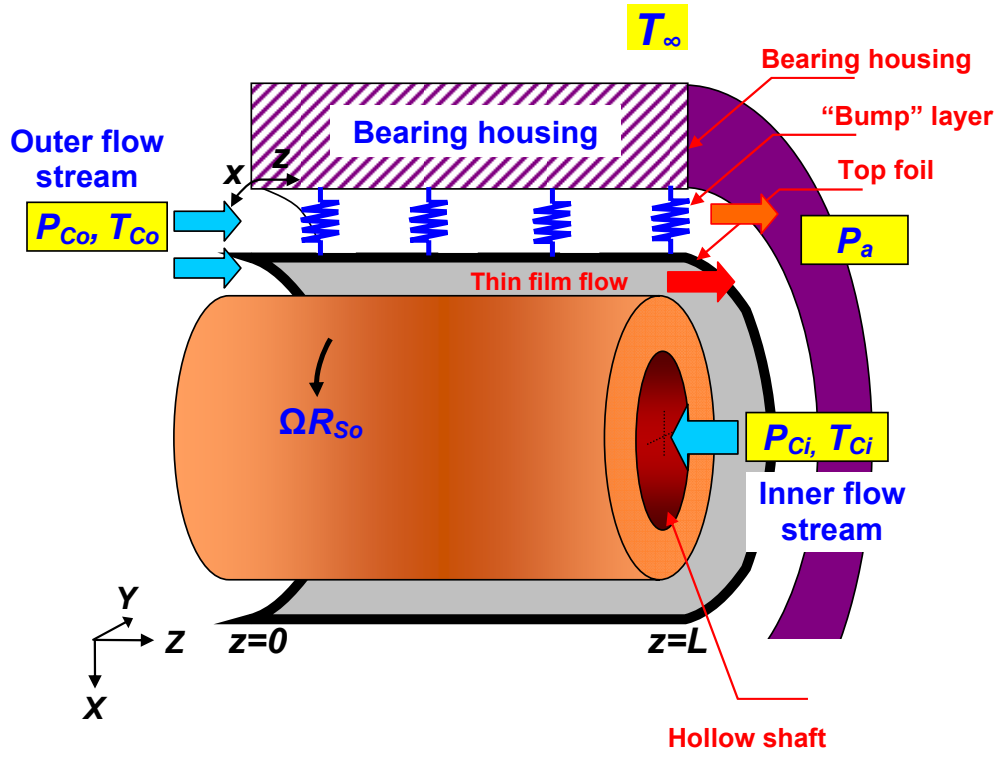

(b) Side view (opened-up view)

Figure 1. Schematic view of cooling flows in gas foil bearing: inner cooling stream (T_{Ci}, P_{Ci}) flows through hollow shaft; and outer cooling stream (T_{Co}, P_{Co}) flows through thin film region and underneath top foil. Outer cooling flow exits to ambient pressure (P_a)

THERMOHYDRODYNAMIC MODEL FOR PREDICTION OF GFB PERFORMANCE

Refer to Figs. 1(a) and 1(b) for a geometrical depiction of the foil bearing, coordinate systems, and nomenclature for the cooling streams, inner and outer. Figure 2 shows the nomenclature for the temperatures in the gas foil bearing and shaft system. Consider:

a) Ideal gas with density $\rho = P / \Re_g T$, where P and T denote absolute pressure and temperature, and $\Re_g$ is the gas constant.

b) Gas viscosity (μ) is a function of absolute temperature only, i.e. $\mu = \alpha_v T$.

c) Gas Specific heat (c_p) and thermal conductivity (κ_g) determined at an effective temperature and regarded as invariant in the thermal process.

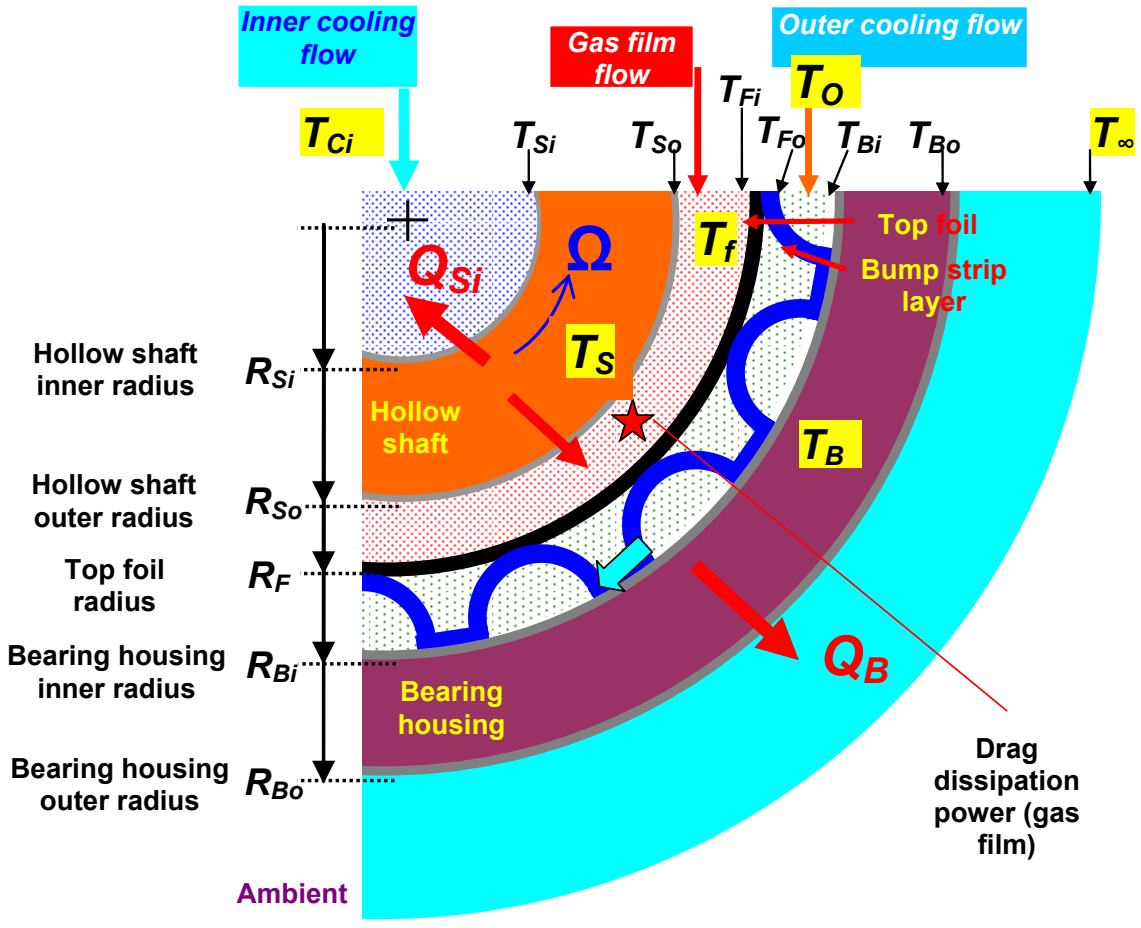

Figure 2. Nomenclature for temperatures in gas foil bearing, hollow shaft, bearing shell, and cooling flow streams

A bulk-flow model describes best the transport of thermal energy [13]. Hence, the noted pressures and temperatures below represent meaningful averages across the film thickness. This assumption is less restrictive for the pressure than for the temperature. The gas flow paths modeled include:

(a) **Thin film gas region**, between rotor surface and top foil, generating the hydrodynamic pressure field $\left(P_{f_{(\Theta,z)}}\right)$ able to support static and dynamic loads. In this region, the gas film temperature $\left(T_{f_{(\Theta,z)}}\right)$ increases due to the dissipation of mechanical energy from viscous drag, and importantly enough, due to convection of heat from the *hot* shaft and carried away by the gas film flow. In addition, some heat also flows into the top foil, part of it advected by the outer flow stream and with the rest conducted into the bearing shell.

(b) **Outer cooling flow stream region** supplied axially at one bearing end with feed conditions $\left(T_{C_o}, P_{C_o}\right)$. This cooling stream increases in temperature $\left(T_{O(\Theta,z)}\right)$, as it removes heat from the back surface of the top foil; while its pressure $\left(P_{O(\Theta,z)}\right)$ decreases toward ambient pressure P_a, as it exits the other end of the bearing ($z=L$).

(c) **Inner cooling flow stream region** at uniform *cold* temperature $\left(T_{C_i}\right)$ In this region, typically of a large diameter, enough gas flow is supplied so that its temperature does not vary along the axial direction.

Hydrodyancmic pressure and tempearure transport with thin film gas flow region

The gas film thickness $\left(h_{f_{(\Theta,z)}}\right)$ separating the rotor from the top foil is very small compared to the shaft outer radius $\left(R_{S_o}\right)$ and bearing axial length (L). Furthermore, the gas kinematic viscosity ($\upsilon=\mu/\rho$) is relatively large, and hence the flow regime within the gas film region is typically laminar and not influenced by fluid inertia. That is, the characteristic Reynolds number based on shaft angular speed (Ω) is relatively small, i.e. $\mathrm{Re}_h^* = \dfrac{\Omega h_f^2}{\nu} < 1$.

Under these considerations, the steady state, laminar flow Reynolds equation for an ideal gas of density $\rho_f = {P_f}/{\Re_g T_f}$ flowing within a thin film thickness h_f is

$$\frac{\partial}{\partial x}\left(\frac{h_f^3 P_f}{12\mu_f \Re_g T_f}\frac{\partial P_f}{\partial x} \right) + \frac{\partial}{\partial z}\left(\frac{h_f^3 P_f}{12\mu_f \Re_g T_f}\frac{\partial P_f}{\partial z} \right) = U_{m(z)}\frac{\partial}{\partial x}\left(\frac{P_f h_f}{\Re_g T_f} \right) \tag{1}$$

where $U_m(z) = \dfrac{\Omega R_{S_o}}{2}\left(1 - e^{-\delta z}\right) + \alpha_\Omega \Omega R_{S_o} e^{-\delta z}$ with $\delta = \dfrac{12\mu_f}{(\dot{m}_z h^2)_f}$ is the mean circumferential flow velocity [14,15], proportional to shaft surface speed and evolving in the axial direction due to the imposed pressure gradient from the outer cooling flow. Above, α_Ω is an empirical inlet flow pre-swirl factor. (x, z) are the circumferential and axial coordinates on the plane of the bearing. $\Re_g$ is the gas constant, and the gas viscosity $\mu = \mu(T)$ is a function of the gas absolute temperature.

For a perfectly aligned journal, the film thickness (h_f) in a GFB with a mechanical preload (r_p) at an offset angle (Θ_p) is [4];

$$h_f = c - r_p \cos\left(\Theta - \Theta_p\right) + e_X \cos(\Theta) + e_Y \sin(\Theta) + w_d \tag{2}$$

where, c, e_X, e_Y, and w_d are the bearing radial clearance, journal center displacements (e_X, e_Y) and top foil elastic deflection, respectively. See Fig. 3 for the geometry of a journal and arcuate top foil with mechanical preload, and their disposition in the Cartesian coordinate system (X ,Y).

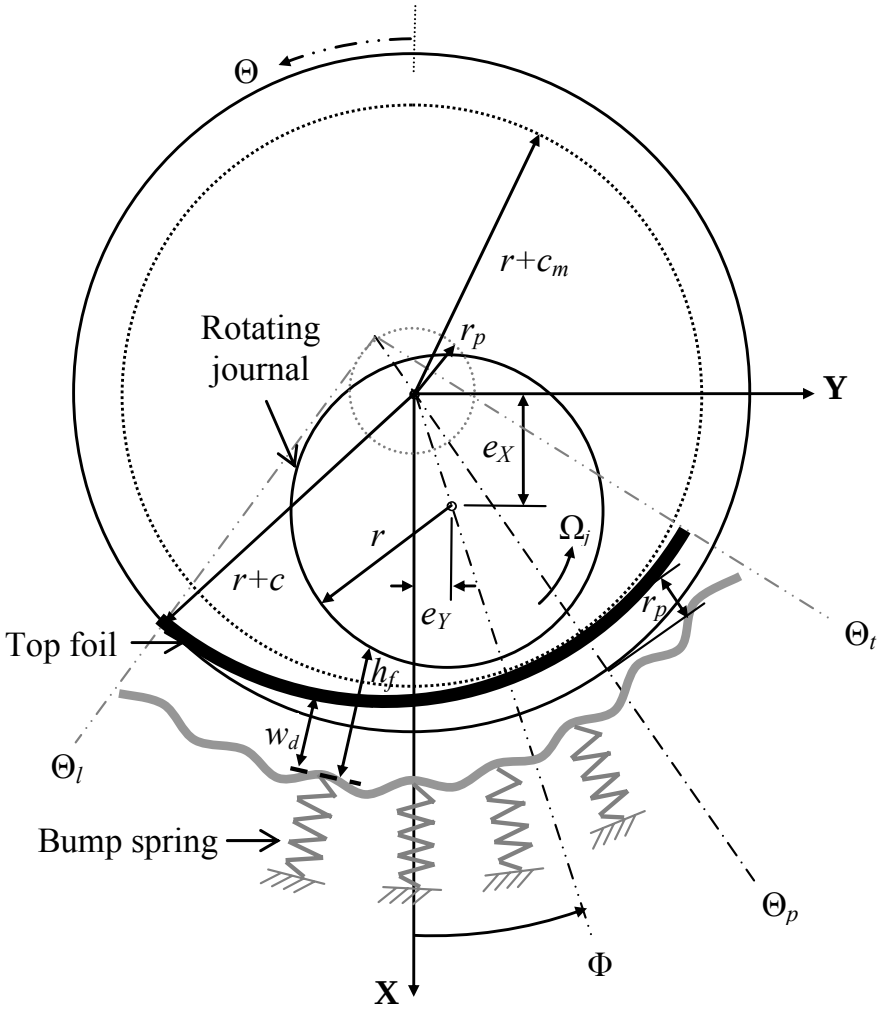

$r_p = c - c_m$
$r_p = 0$: Null preload
$r_p = c$: Journal – top foil contact

c: Radial (foil) clearance
c_m: Assembled radial clearance
h_f: Local film thickness considering, local aerofoil deflection, w_d

Figure 3. Geometry of a journal and arcuate top foil with mechanical preload

The numerical solution of Reynolds Eq. (1) implements a control volume – finite difference scheme with the exact advection model, Ref. [16], ensuring numerical accuracy and stability for operation at high journal rotational speeds, in particular.

The bulk-flow temperature transport equation is derived from integration across the film thickness of the 3D thermal energy transport equation as given in Ref. [13].

$$c_{p_f}\left(\frac{\partial\left(\rho_f h_f U_f T_f\right)}{\partial x}+\frac{\partial\left(\rho_f h_f W_f T_f\right)}{\partial z}\right)+\bar{h}_{fF}\left(T_f-T_{F_i}\right)-\bar{h}_{Sf}\left(T_{S_o}-T_f\right)$$
$$=\left(U_f h_f\frac{\partial P_f}{\partial x}+W_f h_f\frac{\partial P_f}{\partial z}\right)+\frac{12\mu_f}{h_f}\left\{W_f{}^2+\frac{1}{3}U_m+\left(U_f-U_m\right)^2\right\} \qquad (3)$$

Convection of heat by fluid flow + diffusion to bounding surfaces = compression work + dissipated energy

where $\bar{h}_{Sf}$ and $\bar{h}_{fF}$ are the heat fluxes per unit area from shaft into the inner film and from inner film into the top foil front surface, respectively. Above, T_f, T_{S_o} and T_{F_i} are the thin film gas flow temperature, journal outer surface temperature, and the top foil inner surface temperature, respectively. Typically, a heat convection coefficient $\bar{h}$ is a function of the flow conditions (laminar or turbulent), gas thermal conductivity, and a characteristic diffusivity length, i.e. film thickness. (U_f, W_f) are the film flow velocity components along the circumferential and axial direction, respectively, and determined from the momentum transport equations. c_{p_f} denotes the gas specific heat, and gas density $\rho_f = P_f \big/ \Re_g T_f$.

Appendix A details numerical discretization and solution procedure of the governing equations (1,3) for thermohydrodynamic analysis of GFBs, and Appendix B presents the evaluation of the heat convection coefficients for heat transport from the gas film into the rotating shaft and the outer bearing housing.

The **boundary conditions** for the inner film gas pressure and temperature fields $\{P_f, T_f\}$ are[2]:

(a) at the inlet plane $z=0$, $\{\Theta_l \le \Theta \le \Theta_t\}$

$$P_f(\Theta,0,t)=P_{C_o};\ T_f(\Theta,0,t)=T_{C_o} \qquad (4)$$

[2] Reynolds equation for the pressure field is of elliptic type, thus requiring of boundary conditions on the entire closure of the flow domain. On the other hand, the temperature transport equation is of parabolic type with specified boundary conditions at the inlet plane(s) where gas flow is supplied.
In addition note that due to the asymmetry in temperature conditions, an assumed pressure field symmetric about the bearing midplane, i.e. *Pf(z+ ½ L)= Pf(z)* when *0<z< ½ L* , is physically impossible. Prior analyses, see Ref. [7] for example, use this incorrect assumption.

where $\left(P_{C_o}, T_{C_o}\right)$ are the pressure and temperature of the *outer* cooling stream supplied at one end of the GFB.

(b) at the leading edge angle (Θ_l) of top foil, for $\{0 \le z \le L\}$,

$$P_f\left(\Theta_l, z, t\right) = P_O(\Theta_l,\ z); \quad T_f\left(\Theta_l, z, t\right) = T_{f_l}(\Theta_l) \tag{5}$$

with $T_{f_l} = f\left(T_O\left(\Theta_l\right), T_f\left(\Theta_t, z, t\right)\right)$, and $\{P_O, T_O\}$ as the gas pressure and temperature underneath the top foil (outer flow cooling stream).

(c) at the trailing edge angle (Θ_t) of top foil, for $\{0 \le z \le L\}$,

$$P_f\left(\Theta_t, z, t\right) = P_O(\Theta_t, z) \tag{6}$$

with the *exit* temperature leaving the topfoil, $T_{f_e} = T_f\left(\Theta_t, z, t\right)$, determined by solving Eq. (5).

Note that the inlet temperature T_{f_l} at the top foil leading edge (Θ_l) results from mixing of a fraction of the *hot* film stream leaving the top foil with temperature T_{f_E} with the externally supplied cold outer stream flow at temperature $T_{O(z)}$.

(d) at the exit plane, $z=L$, $\{\Theta_l \le \Theta \le \Theta_t\}$

$$P_f\left(\Theta, L, t\right) = P_a \tag{7}$$

where P_a denotes ambient temperature. The exit film temperature $T_f\left(\Theta, L, t\right)$ is determined from solution of the thermal energy transport Eq. (3).

PREDICTIONS OF GAS FILM PRESSURE AND TEMPERATURE FIELDS

Model predictions follow for a generation I GFB with axial length L and diameter D equal to 38.1 mm. The bearing housing and bump dimensions studied are identical to those of a GFB tested in Ref. [4]. Table 1 displays the bearing geometry and operating conditions for the GFB studied. Ambient conditions are noted as 25 °C and 1 bar in pressure.

Table 1. Geometry and operating conditions of Generation I GFB

Parameters	Values
Bearing radius, $R=D/2$	19.05 mm
Bearing length, L	38.1 mm
Foil arc circumferential length, l_x	120 mm
Nominal radial clearance, c	70 μm
Top foil thickness, t_t	102 μm
Bump foil thickness, t_b	102 μm
Bump pitch, s_0	4.572 mm
Bump half length, l_0	2.032 mm
Bump height, h_b	0.381 mm
Number of bumps, N_b x strips, N_s	25 x 1
Bump foil Young's modulus at 25 °C, E	213 GPa
Bump foil Poisson's ratio, v	0.29
Bump foil stiffness, k_B	3.16 GN/m^3
Gas properties	Air
Gas Constant, $\Re_g$	286.7 J/(kg-K)
Viscosity, μ	1.85×10^{-5} Pa-s
Conductivity, κ	0.0257 W/m.K
Density, ρ	1.169 kg/m^3
Specific heat, c_p	1,020 J/kg.K
Ambient pressure, P_a	1.014 x 10^5 Pa
Ambient temperature, T_a	25 °C (298 K)

The gas properties in Table 1 are nominal at room temperature (25 °C). Note that gas viscosity (μ) and conductivity (κ) change with gas temperature. Appendix C provides the air material properties (μ) and (κ) versus temperature, as implemented in the analysis program. Figures C1 and C2 include predictive formulas, where (x) and (y) denote the variables in the horizontal and vertical axes, respectively. The linear fit correlation coefficients (R^2) are close to unity. Note that gas specific heat (c_p) is taken as a constant (1,020 J/kg K) since it does not change significantly with temperature. For example, c_p varies from 1,005 J/kg K at -150 °C to 1,067 J/kg K at 400 °C [17].

Note that, in Appendix D, predictions of shaft centrifugal growth and thermal expansion for increasing rotor speeds and temperatures show a significant reduction in the nominal radial clearance (c = 70 μm in Table 1) during rotor operation.

The current analysis assumes an ambient (or supply) air temperature T_{supply} = 25 °C. The whole bearing housing surface is at 25 °C, and the shaft temperature varies from 25 °C to 150 °C. Hence, the thermal gradient is from the hot shaft to the bearing housing.

Note that top foil detachment doest not allow for sub-ambient pressures [3]. Thus, ingress of (fresh or cold) air flow from the axial sides of the bearing into the gas film is unlikely to occur. In reality, fresh gas flow is naturally drawn into the thin film at the largest gap between the top foil leading and trailing edges. Hence, an adequate thermal energy and flow mixing condition[3] occurs at this location.

Figure 4 presents the predicted (a) film pressure P_f and (b) bulk-flow film temperature T_f fields for the GFB operating at a rotor speed of 40,000 rpm. A static load of 5 N is applied toward 180° (vertical downwards – along X direction, see Fig. 1). The shaft surface temperature (T_S) is at 25 °C and no feed cooling gas flow is supplied. The predicted journal eccentricity, journal attitude angle, and minimum film thickness are 26.6 μm, 60°, and 42.3 μm, respectively. Along the circumferential coordinate, $0 < \theta < 200$ °, the film temperature increases as the gas flows and removes the shear induced mechanical energy. However, for $\theta > 200$ °, the temperature drops due to (a) the gas expansion - reduction in pressure – that cools the gas film, and (b) due to the negligible shear dissipation energy - further downstream- once the top foil detaches. The prediction shows that the inlet gas film temperature at the top foil leading edge increases slightly from 25 °C to 25.5 °C[4], while the peak temperature of ~29 °C occurs at the bearing mid-plane, just downstream of the peak film pressure ~200 °. Note that the simple Couette flow approximation [6,18] predicts a peak temperature at the top foil trailing edge and underestimates the actual peak film temperature, in particular for heavily loaded GFBs. This

[3] λ denotes the fraction of upstream gas flow (trailing edge of top foil) re-entering the thin film of the GFB at the leading edge of the top foil. Note that $\dot{m}_{Rec} + \dot{m}_{Supply} = \dot{m}_{inlet}$; $\dot{m}_{Rec} = \lambda\, \dot{m}_{up}$ where $\dot{m}_{Rec}$, $\dot{m}_{Supply}$, $\dot{m}_{Inlet}$, and $\dot{m}_{up}$ are recirculation flow, fresh supply flow, inlet film flow, and, upstream flow at the trailing edge, respectively. A simple thermal energy balance, i.e., $\dot{m}_{Rec}T_{Rec} + \dot{m}_{Supply}T_{Supply} = \dot{m}_{Inlet}T_{Inlet}$ leads to $T_{Inlet} = \left(\dot{m}_{Rec}T_{Rec} + \dot{m}_{Supply}T_{Supply}\right)\big/\dot{m}_{Inlet}$. The thermal inlet mixing ratio λ (<1) depends on the bearing configuration and applied cooling method.

[4] The inlet mixing flow temperature is found iteratively using the calculated recirculation flow temperature and the fresh air supply flow temperature of 25 °C with a mixing ratio λ which satisfies $\dot{m}_{Rec} = 0.5\dot{m}_{Inlet}$.

approximation is strictly valid for operation at small journal eccentricities and ignores the effects of gas compressibility.

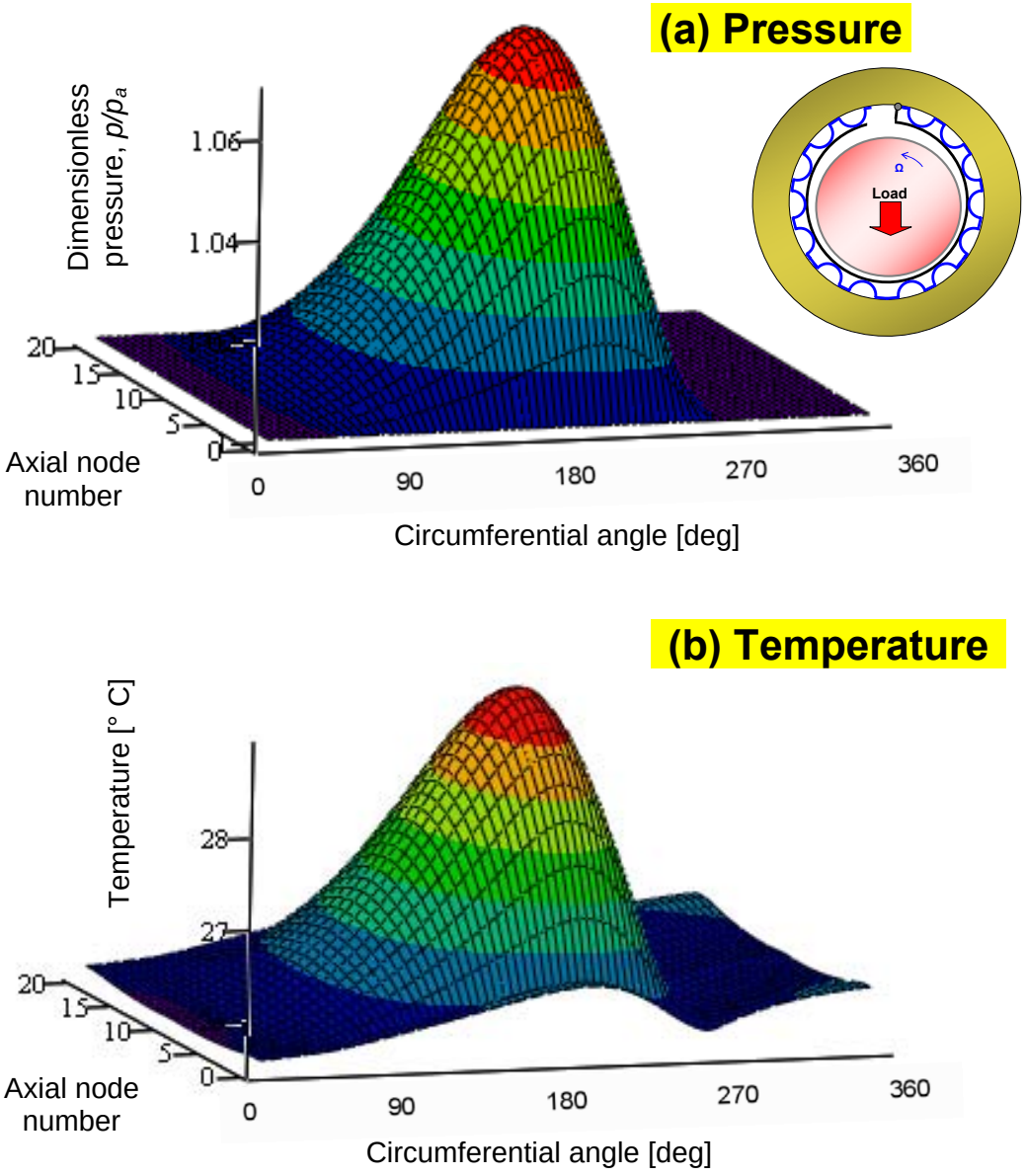

Figure 4. Predicted gas film (a) pressure and (b) temperature fields in a GFB operating at a rotor speed of 40,000 rpm. Static load of 5 N applied toward 180°. Supply air (T_{supply}), shaft (T_S), and bearing housing (T_B) temperatures at 25 °C. No axial cooling gas flow

The following results refer to thermal boundaries (a) insulated or adiabatic walls, i.e. no heat transfer to/from the bounding walls and, (b) heat convection/conduction from hot shaft into gas film and heat conduction from gas film into bearing cartridge at 25 ºC.

Figure 5 shows predicted gas film peak temperature versus static load at a rotor speed of 40,000 rpm for an adiabatic walls condition and for heat convection to the bounding walls, i.e. shaft and top foil. In general, predictions show that the peak temperature, which occur along the bearing mid-plane, increases as the static load increases. Differences in the magnitudes between the two model predictions increase significantly as static load increases. The difference in the peak temperature of 2 ºC (= 31 ºC - 29 ºC) with a static load of 5 N increases to 34 ºC (= 89 ºC - 55 ºC) with a static load of 75 N, for example.

Figure 6 depicts predicted journal eccentricity and minimum film thickness versus static load at a rotor speed of 40,000 rpm for the adiabatic walls condition and for the heat convection to/from the bounding walls. The figure also shows predictions from an isothermal flow model [3]. The isothermal flow model neglects altogether the thermal energy transport and assumes a constant gas film temperature (T_f=T_{supply}). As the static load increases, the predicted journal eccentricity increases and the minimum film thickness decreases. The isothermal flow model predicts the largest journal eccentricity and the smallest minimum film thickness, while the adiabatic walls model predicts the smallest journal eccentricity and the largest minimum film thickness. For the adiabatic walls model, the increase in the gas film temperature (max. ~ 85 °C) increases the gas viscosity (~14.3 %); see Appendix C, thus leading to the increase in the minimum film thickness. Note that current model predictions do account for the change in the modulus of elasticity for the underlying foil material (Inconel X750) due to the increase in the gas film temperature. However, the effect of the change in the material modulus of elasticity on the bearing performance is insignificant with the moderate increase in the film temperature. Appendix E shows that the modulus of elasticity for the Inconel X750 material decreases by ~1.7% with temperature increasing to 85 °C, for example.

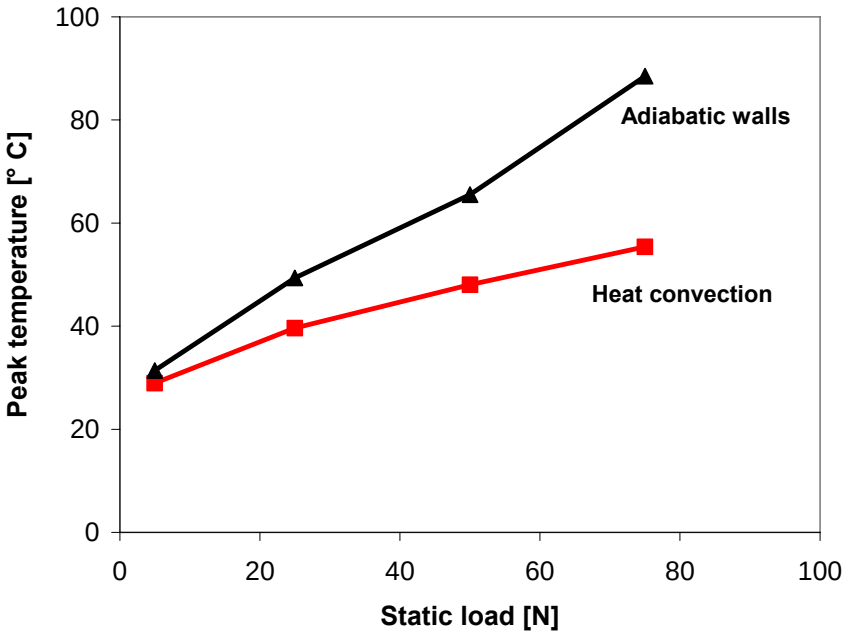

Figure 5. Predicted gas film peak temperature versus static load for adiabatic walls condition and for heat convection to bounding walls at a rotor speed of 40,000 rpm. Supply air (T_{supply}), shaft (T_S), and bearing housing (T_B) temperatures at 25 °C. No axial cooling gas flow

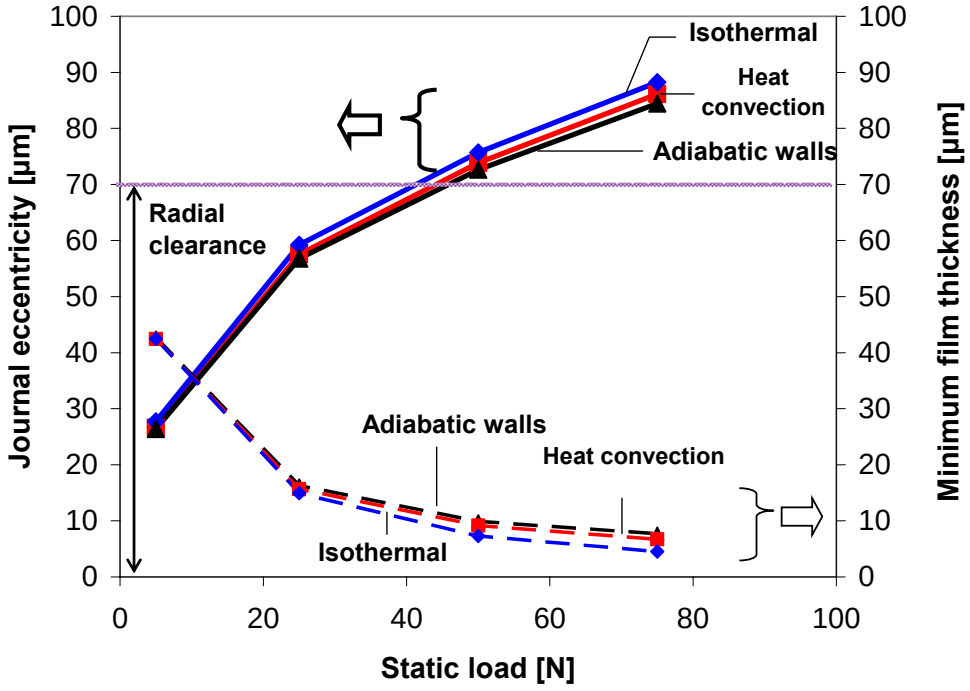

Figure 6. Predicted journal eccentricity and minimum film thickness versus static load for isothermal flow, for adiabatic walls condition, and for heat convection to bounding walls at a rotor speed of 40,000 rpm. Supply air (T_{supply}), shaft (T_S), and bearing housing (T_B) temperatures at 25 °C. No axial cooling gas flow

Figure 7 shows predicted gas film peak temperature versus rotor speed for increasing shaft temperatures from 25 °C to 150 °C. The predictions account for heat transfer from the journal and to the bearing housing surface, at constant temperature of 25 ºC. The static load is 5 N and no cooling gas flow is supplied. As the shaft temperature increases, the gas film peak temperature also increases. The gas film has a lower temperature than the shaft since heat flows from the shaft to the outer bearing housing and due to the mixing of the recirculation film flow with the ingress of fresh air at the top foil leading edge. For the shaft temperature of 25 °C, the gas film temperature increases as the rotor speed increases. On the other hand, the film temperature decreases with increasing rotor speeds for the higher shaft temperatures. As the rotor speed increases, the ingress of fresh air into the bearing clearance increases, thus decreasing the film peak temperature, in particular for high shaft temperatures.

Figure 8 shows the predicted shaft thermal expansion versus shaft temperature. As the shaft temperature increases from 25 °C to 150 °C, the shaft thermal expansion increases linearly to 30 μm, i.e., ~ 43 % of the nominal radial clearance of 70 μm.

Figure 9 shows the predicted actual (operating) radial clearance versus rotor speed. The actual radial clearance is calculated by subtracting the shaft thermal expansion, shown in Fig. 8, and centrifugal growth from the nominal radial clearance of 70 μm. Note that the shaft centrifugal growth, which is a function of a rotor speed and component material properties, is 1.8 μm at the maximum rotor speed of 50 krpm. At 50 krpm, as the shaft temperature increases to 150 °C, the bearing radial clearance reduces dramatically to ~38.2 μm.

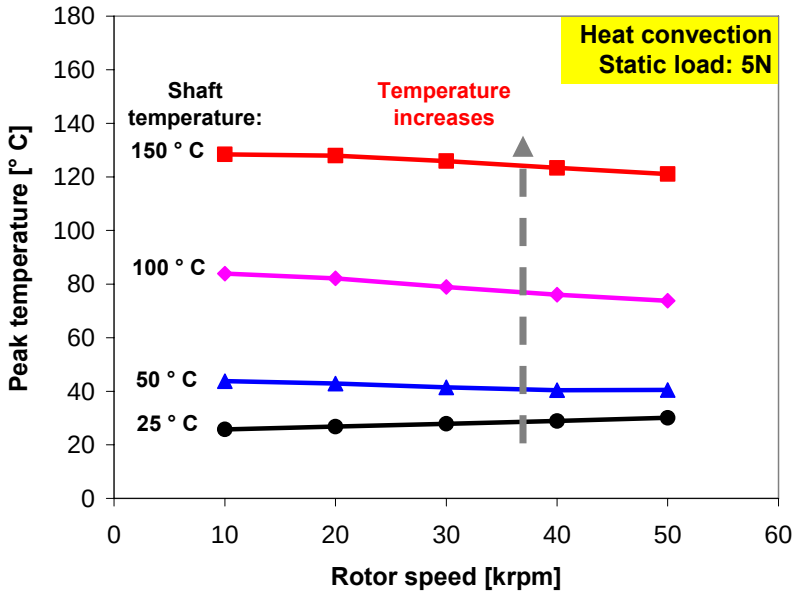

Figure 7. Predicted gas film peak temperature versus rotor speed for operation with increasing shaft temperatures (T_S) at 25 °C, 50 °C, 100 °C, 150 °C. Supply air (T_{supply}) and bearing housing temperature (T_B) at 25 °C. Static load of 5 N. No axial cooling gas flow

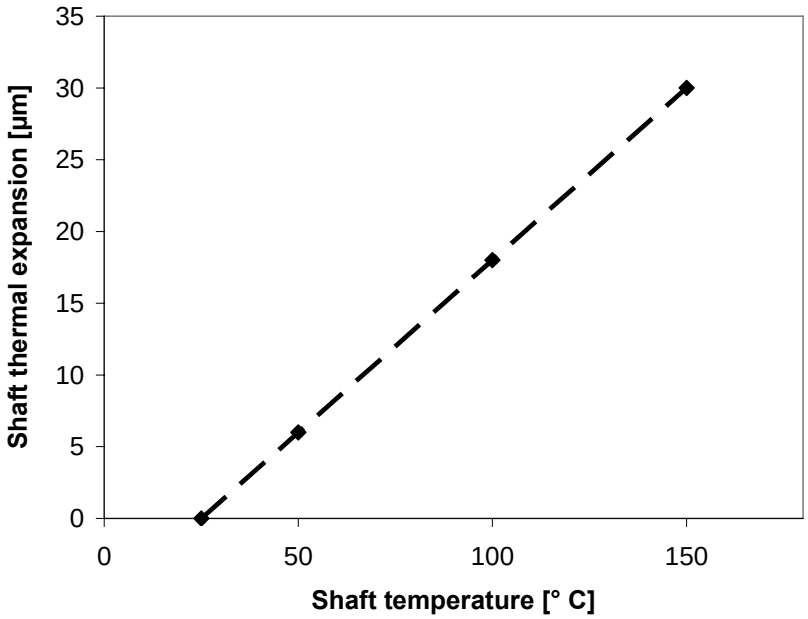

Figure 8. Predicted shaft thermal expansion versus shaft temperature

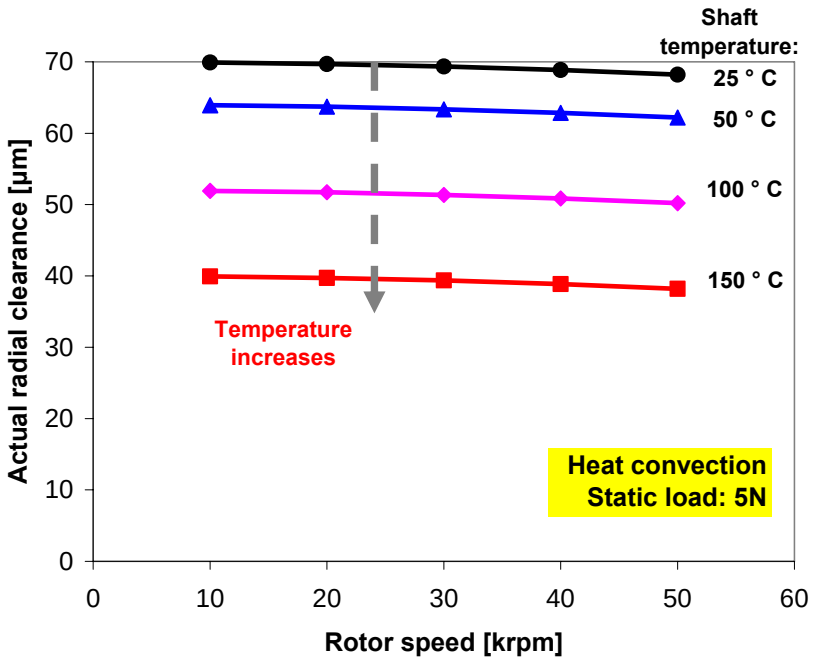

Figure 9. Predicted actual radial clearance versus rotor speed for operation with increasing shaft temperatures (T_S) at 25 °C, 50 °C, 100 °C, 150 °C. Supply air (T_{supply}) and bearing housing temperature (T_B) at 25 °C. Static load of 5 N. No axial cooling gas flow

Figure 10 shows the predicted journal eccentricity and minimum film thickness versus rotor speed for increasing shaft temperatures and a low static load of 5N. As the rotor speed increases, the journal eccentricity decreases and the minimum film thickness increases. As the shaft temperature increases, the journal eccentricity decreases. The minimum film thickness increases with temperature at low rotor speed but decreases with temperature at high rotor speeds. Note that both the increase in gas viscosity and the decrease in actual bearing clearance, due to temperature rise, ultimately affect the minimum film thickness.

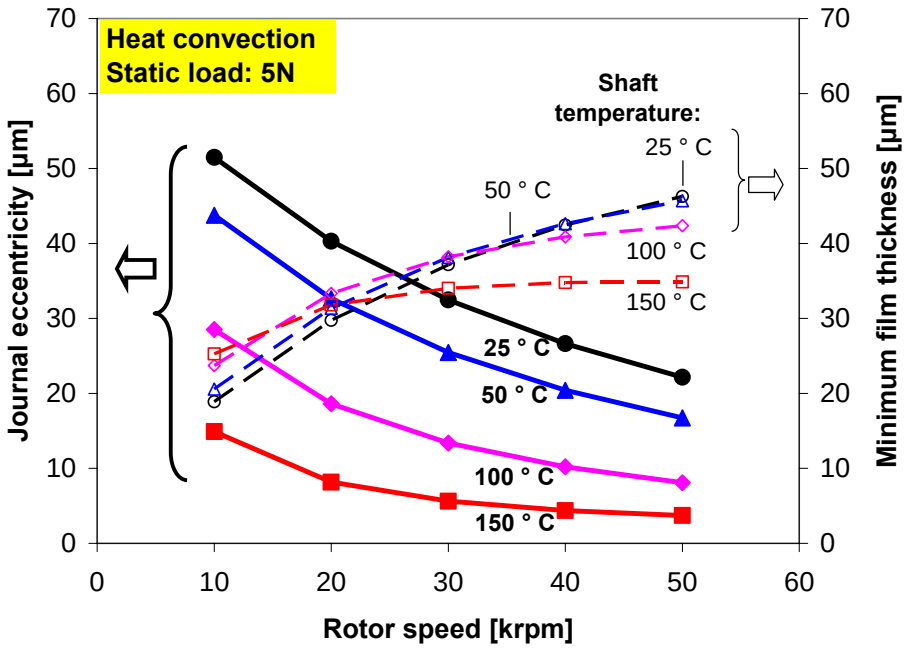

Figure 10. Predicted journal eccentricity and minimum film thickness versus rotor speed for operation with increasing shaft temperatures (T_S) at 25 °C, 50 °C, 100 °C, 150 °C. Supply air (T_{supply}) and bearing housing temperature (T_B) at 25 °C. Static load of 5 N. No axial cooling gas flow

Figure 11 shows the predicted journal attitude angle versus rotor speed for operation with increasing shaft temperatures. For a shaft at temperatures < 150 °C, the journal attitude angle increases as the rotor speed increases, while it is nearly constant for a shaft at temperatures of 150 °C above 20 krpm. In general, at rotor speeds < 50 krpm, the journal attitude angle increases significantly as the shaft temperature increases but the journal has a nearly constant attitude angle at a high rotor speed of 50 krpm.

In Fig. 12, the predicted bearing drag torque increases linearly as the rotor speed increases. An increase in shaft temperature increases the gas viscosity and reduces the bearing actual clearance, thus resulting in the increase in the bearing drag torque, in particular at high rotor speeds.

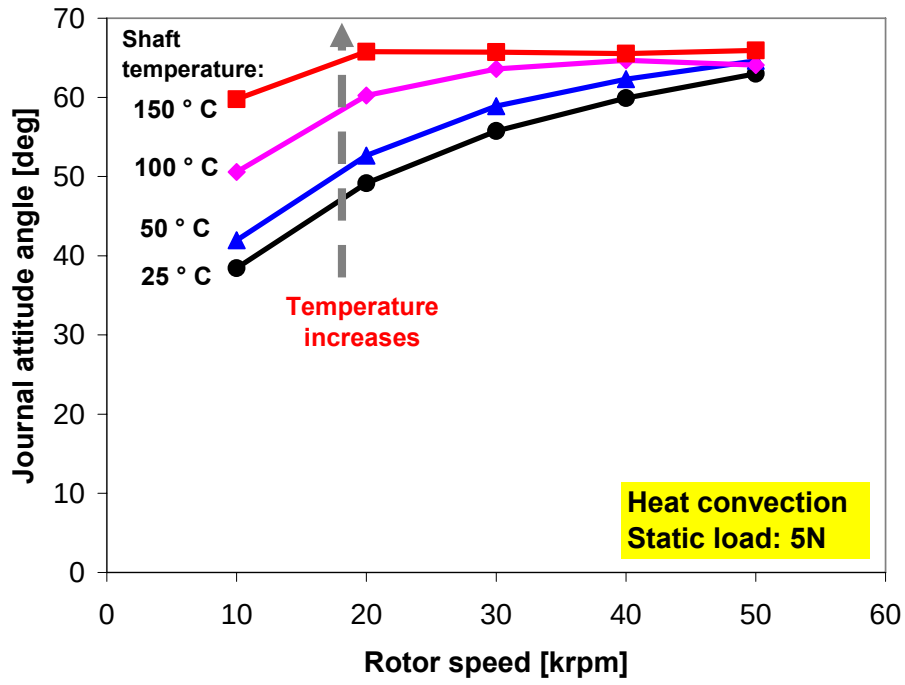

Figure 11. Predicted journal attitude angle versus rotor speed for operation with increasing shaft temperatures (T_S) at 25 °C, 50 °C, 100 °C, 150 °C. Supply air (T_{supply}) and bearing housing temperature (T_B) at 25 °C. Static load of 5 N. No axial cooling gas flow

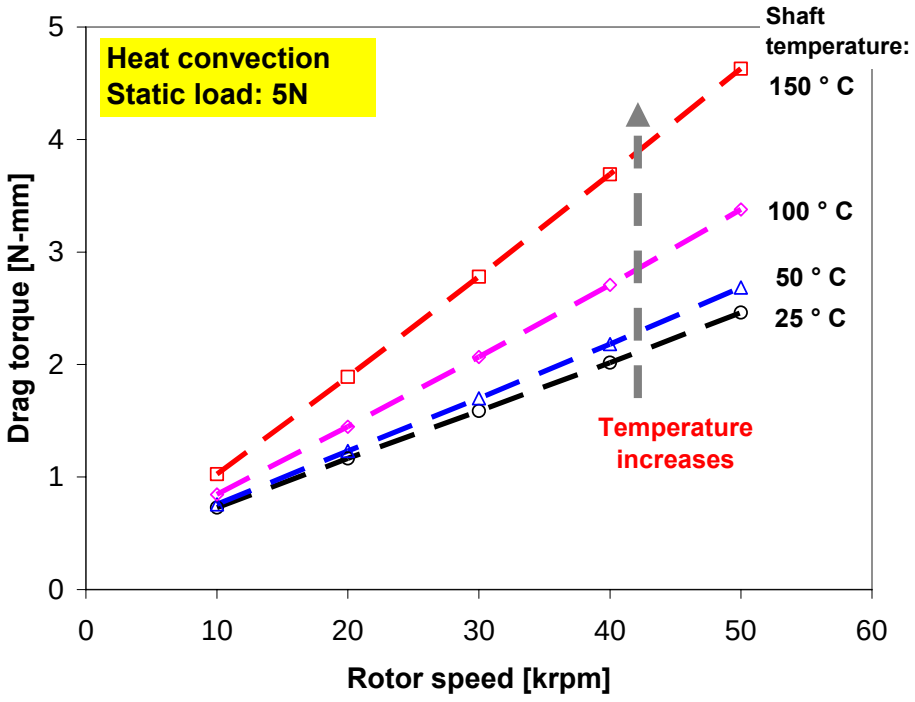

Figure 12. Predicted bearing drag torque versus rotor speed for operation with increasing shaft temperatures (T_S) at 25 °C, 50 °C, 100 °C, 150 °C. Supply air (T_{supply}) and bearing housing temperature (T_B) at 25 °C. Static load of 5 N. No axial cooling gas flow

When a cooling gas flow is forced through the foil bearing underlying structure to carry away heat from a hot shaft and mechanical energy dissipated within the gas film, an equivalent heat transfer coefficient $\bar{h}_{eq}$ represents a multilayer conduction/convection. See Appendix B for the definition of $\bar{h}_{eq}$, which also includes a heat transfer coefficient for an outer cooling flow stream $\bar{h}_{FO}$.

Figure 13 shows predicted gas film peak temperature versus axial cooling flow for increasing static loads at a rotor speed of 40,000 rpm. The supply (ambient) air and cooling air temperature $T_{supply} = T_{cooling} = 25$ °C. The shaft and bearing outer surface temperature $T_S = T_{BO} = 150$ °C. The peak temperature decreases, as the cooling flow increases and as the static load increases. The predictions imply that an adequate thermal management using a (limited) cooling flow takes away heat from the back of the top foil and controls the gas film temperature. However, note that the rate of decrement in the predicted peak temperature reduces as the cooling flow increases.

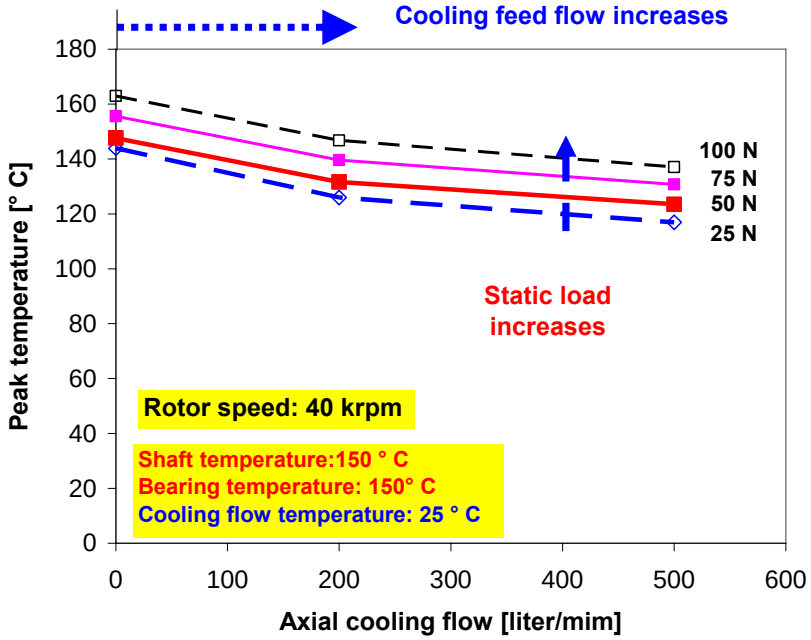

Figure 13. Predicted peak film temperature versus axial cooling flow for increasing static loads. Rotor speed of 40,000 rpm. Supply air and cooling air temperature ($T_{supply} = T_{cooling}$) at 25 °C, shaft and bearing outer surface temperature ($T_S = T_{BO}$) at 150 °C

CLOSURE

A compressive thermohydrodynamic model of GFBs does not only account for thermal energy transport within the gas film region but must also include detailed heat flux paths from the gas film to the bearing housing and into the shaft. This report details the gas film pressure (Reynolds) and temperature transport equations in a GFB and the calculation of the overall (equivalent) heat transfer coefficients representing heat transfer from/into the thin film into/from the rotating shaft and the top foil and heat conduction through the bump strip layer and into/from the bearing housing. The model equations estimate the actual foil bearing clearance from thermoelastic relations depending on material properties, rotor speed and components' thermal growth.

Predictions show a peak gas film temperature at the bearing mid-plane and just downstream of the peak film pressure. As the static load increases, the film peak temperature also increases. For the shaft and the bearing housing at constant room temperature of 25 ºC, the predicted THD minimum film thickness (or load capacity) is larger than that from an isothermal flow model due to the increase in the gas viscosity with temperature. The THD minimum film thickness is smaller than that for an adiabatic walls condition. An increase in the shaft temperature and shaft thermal expansion decreases significantly the bearing operating clearance, thus resulting in a decrease of the minimum film thickness and the journal eccentricity, in particular at high rotor speeds. The bearing drag torque increases with shaft temperature due to an increase in the gas viscosity and a decrease in the bearing operating clearance. Implementation of axial cooling flow through the GFB enhances heat convection, thus decreasing peak temperatures.

The present study demonstrates that adequate thermal management aids to control the bearing operating clearance and enhances the load capacity for operation in high temperature environment. Implementation of a cooling flow through GFBs decreases the gas film temperature, thus reducing the likelihood of thermal seizure and bearing failure. In addition, an engineered thermal expansion of the bearing cartridge (with a large thermal expansion coefficient) can help to compensate for a reduction in the bearing clearance.

REFERENCES

[1] DellaCorte, C., and Valco, M. J., 2000, "Load Capacity Estimation of Foil Air Journal Bearings for Oil-Free Turbomachinery Applications," NASA/TM, Report No. 2000-209782.

[2] Heshmat, H., 1994, "Advancements in the Performance of Aerodynamic Foil Journal Bearings: High Speed and Load Capacity," ASME J. Tribol., **116**, pp. 287–295.

[3] Kim, T. H., and San Andrés, L., 2008, "Heavily Loaded Gas Foil Bearings: a Model Anchored to Test Data," ASME J Gas Turbines Power, **130**, 012504.

[4] Kim, T. H., 2007, "Analysis of Side End Pressurized Bump Type Gas Foil Bearings: A Model Anchored to Test Data," Texas A&M University, Ph. D. Dissertation, College Station, TX.

[5] Radil, K., DellaCorte, C., Bruckner, R., and Zessoteck, M., 2007, "Thermal Management Techniques for Oil-Free Turbomachinery Systems," STLE Tribol. Trans., **50**, pp. 319-327

[6] Salehi, M., Swanson, E., and Heshmat, H., 2001, "Thermal Features of Compliant Foil Bearings – Theory and Experiments," ASME J. Tribol., **123**, pp. 566-571.

[7] Peng, Z-C., and Khonsari, M. M., 2006, "A Thermohydrodynamic Analysis of Foil Journal Bearings," ASME J. Tribol., **128**, pp. 534-540.

[8] Radil, K. C. and Zeszotek, M., 2004, "An Experimental Investigation into the Temperature Profile of a Compliant Foil Air Bearing," STLE Tribol. Trans., **47**(4), pp 470-479.

[9] Le Lez, S., 2007, "Caracterisques Statiques Et Dynaniques Des Paliers A Feuilles," Ph.D. Dissertation, Universite De Poitiers, France.

[10] Feng, K., and Kaneko, S., 2008, "A Study of Thermohydrodynamic Features of Multiwound Foil Bearing Using Lobatto Point Quadrature," ASME Paper No. GT2008-50110.

[11] Sim, K., and Kim, D., 2008, "Thermohydrodynamic Analysis of Compliant Flexure Pivot Tilting Pad Gas Bearings," ASME J Eng. Gas Turbines Power, **130**(5), 032502.

[12] Lubell, D., DellaCorte, C. and Stanford, M.: "Test Evolution and Oil-Free Engine Experience of a High Temperature Foil Air Bearing Coating," ASME Paper No. GT2006-90572.

[13] San Andrés, L., 2007, "Thermohydrodynamic Bulk-Flow Model in Thin Film Lubrication," Lecture Notes # 10 in Modern Lubrication Theory, available at http://phn.tamu.edu/me626

[14] Black, H. F., Allaire, P. E., and Barrett, L. E., 1981, "Inlet Flow Swirl in Short Turbulent Annular Seal Dynamics," *Proc. 9th Intl. Conf. in Fluid Sealing*, BHRA Fluid Engineering, Leeuwenborst, The Netherlands, pp. 141-152.

[15] Childs, D., 1993, *Turbomachinery Rotordynamics*, John Wiley & Sons, Inc., NY, Chapter 4, pp. 239-259.

[16] Faria, M., and San Andrés, L., 2000, "On the Numerical Modeling of High speed Hydrodynamic Gas Bearing," ASME Journal of Tribology, **122**, pp 124-130.

[17] Air Properties, http://www.engineeringtoolbox.com/air-properties-d_156.html, Accessed February 13, 2008.

[18] Pinkus, O., and Sternlicht, B., 1961, Theory of Hydrodynamic Lubrication, McGraw Hill, New York, pp. 14-22.

[19] Patankar, S. V., 1980, *Numerical Heat Transfer and Fluid Flow*, Hemisphere Publishing Corporation, McGraw Hill.

[20] Whitaker, S., 1977, *Fundamental Principles of Heat Transfer*, Pergamon Press, New York, pp. 208-219.

[21] Holman, J. P., 1990, *Heat Transfer*, McGraw Hill, New York, pp. 245-247.

[22] Bird, R. B., Stewart, W.E., Lightfoot, E.N., 1960, Transport Phenomena, John Wiley & Sons, Inc., New York, pp. 318-323.

[23] Timoshenko, S. P. and Goodier, J. N., 1970, *Theory of Elasticity*, McGraw-Hill, pp. 80-83.

[24] AISI 4140 Steel, http://www.efunda.com/materials/alloys/alloy_steels/show_alloy.cfm?ID=AISI_4140&prop=all&Page_Title=AISI%204140, Accessed April 12, 2008.

[25] Thermal expansion coefficient, http://en.wikipedia.org/wiki/Coefficient_of_thermal_expansion, accessed February, 12, 2008.

[26] Inconel 718, http://www.espimetals.com/tech/inconel718.pdf, Accessed February. 12, 2008.

[27] Inconel X-750 technical data, http://www.hightempmetals.com/techdata/hitempInconelX750data.php, Accessed February. 12, 2008.

[28] Stainless Steel – AISI 304: Material Information, http://www.goodfellow.com/csp/active/STATIC/A/Stainless_Steel_-_AISI_304.HTML, Accessed February 12, 2008.

APPENDIX A: NUMERICAL SOLUTION PROCEDURE FOR GOVERNING EQUATIONS FOR THERMOHYDRODYNAMIC ANALYSIS OF GFBS

The numerical solution of Reynolds Eq. (1) implements a control volume – finite difference scheme with the exact advection model, Ref. [16]. Figure A1 shows the configuration of a control volume. The balance of mass flow rates[5] through the control volume faces equal

$$\dot{M}_e - \dot{M}_w + \dot{M}_n - \dot{M}_s = 0 \tag{A1}$$

where the indices *n, s, e, w* denote the north, south, east and west faces. The mass flow rates are

$$\dot{M}_e = -D_e\left(P_{f_E} - P_{f_P}\right) + U_{m(z)}\frac{h_{f_e}}{\Re_g T_{f_e}}\left(a_e P_{f_P} + b_e P_{f_E}\right)\Delta z \;;$$

$$\dot{M}_w = -D_w\left(P_{f_P} - P_{f_W}\right) + U_{m(z)}\frac{h_{f_w}}{\Re_g T_{f_w}}\left(a_w P_{f_W} + b_w P_{f_P}\right)\Delta z \;; \tag{A2}$$

$$\dot{M}_n = -D_n\left(P_{f_N} - P_{f_P}\right); \qquad \dot{M}_s = -D_s\left(P_{f_P} - P_{f_S}\right)$$

with the following definitions for the diffusion coefficients:

$$D_e = \frac{{h_{f_e}}^3 P_{f_e}}{12\mu_{f_e}\Re_g T_{f_e}} Cl_e\left(\frac{\Delta z}{\Delta x}\right); \; D_w = \frac{{h_{f_w}}^3 P_{f_w}}{12\mu_{f_w}\Re_g T_{f_w}} Cl_w\left(\frac{\Delta z}{\Delta x}\right); \tag{A3}$$

$$D_n = \frac{{h_{f_n}}^3 P_{f_n}}{12\mu_{f_n}\Re_g T_{f_n}} Cl_n\left(\frac{\Delta x}{\Delta z}\right); \; D_s = \frac{{h_{f_s}}^3 P_{f_s}}{12\mu_{f_s}\Re_g T_{f_s}} Cl_s\left(\frac{\Delta x}{\Delta z}\right)$$

and

$$Cl_e = \frac{Cl'_e}{2} = \frac{\lambda_e}{2}\frac{\left(1+e^{\lambda_e}\right)}{\left(e^{\lambda_e}-1\right)}; \; Cl_w = \frac{Cl'_w}{2} = \frac{\lambda_w}{2}\frac{\left(1+e^{\lambda_w}\right)}{\left(e^{\lambda_w}-1\right)}; \; Cl_n = 1; \; Cl_s = 1; \tag{A4}$$

with
$$\lambda_w = \left(\frac{U_{m(z)}\Delta x}{{h_{f_w}}^2 P_{f_w}}\right); \; \lambda_e = \left(\frac{U_{m(z)}\Delta x}{{h_{f_e}}^2 P_{f_e}}\right) \tag{A5}$$

as local *Peclet numbers* defining the flow condition through the faces of the control volume , i.e. the ratio of advection (shear) flow to pressure driven (Poiseuille) flow. The thin film gas

[5] Please note that Reynolds equation is just the mass continuity equation onto which the momentum transport equations for thin film flows are integrated into.

pressures at the interfaces surrounding the control volume are interpolated as

$$P_{f_w} = a_w P_{f_W} + b_w P_{f_P};\ \ P_{f_e} = a_e P_{f_P} + b_e P_{f_E}$$
$$P_{f_s} = a_s P_{f_S} + b_s P_{f_P};\ \ P_{f_n} = a_n P_{f_P} + b_n P_{f_N} \qquad \text{(A6)}$$

where $b's = 1 - a's$ and a is a function of the local *Peclet* number within the respective control volume.

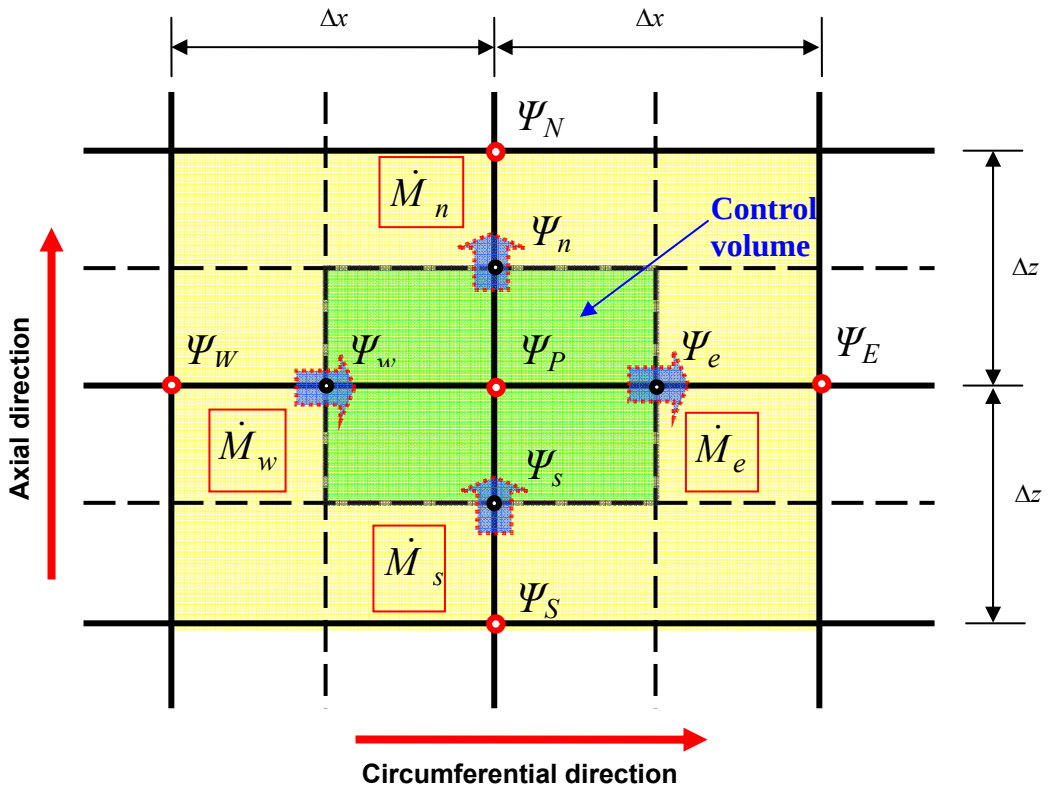

Figure A1. Configuration of control volume for integration of flow equations ($\Psi = P_f$ or T_f). Subscripts *E,W,N,S* for east, west, north, and south nodes; and subscripts *e,w,n,s* for east, west, north, and south faces of control volume

Substituting Eqs. (A3-A6) into Eq. (A1) and arranging leads to an algebraic equation for the nodal pressures:

$$A_w P_{f_W} + B_p P_{f_P} + C_e P_{f_E} - D_n P_{f_N} - D_s P_{f_S} = 0 \tag{A7}$$

where

$$A_w = -D_w - U_{m(z)} \frac{h_{f_w} a_w}{T_{f_w}} \Delta z \;\; ; \quad C_e = -D_e - U_{m(z)} \frac{h_{f_e} b_e}{T_{f_e}} \Delta z \;\; ; \tag{A8}$$

$$B_p = \left(D_e + D_w + D_n + D_s \right) + U_{m(z)} \left(\frac{h_{f_e} a_e}{T_{f_e}} - \frac{h_{f_w} b_w}{T_{f_w}} \right) \Delta z$$

Algebraic Eq. (A7) for the control volume shown in Fig. A1 is solved using the TDM algorithm [19], sweeping along the circumferential direction at a fixed axial (*z)* position. The process is iterative until the found pressure field does not vary within a certain tolerance and also satisfying a minimum mass flow residual within each control volume. After completion of the iterative process, integration of the pressure field on the bearing surface renders the GFB reaction forces [3].

Integration of Eq. (3) on the control volume in Fig. A1 leads to:

$$c_{p_f} \left[\begin{array}{l} \left(\rho_f \, h_f \, U_f T_f \right)^e \Delta z \; - \left(\rho_f \, h_f \, U_f T_f \right)^w \Delta z \\ + \left(\rho_f \, h_f \, U_f T_f \right)^n \Delta x \; - \left(\rho_f \, h_f \, U_f T_f \right)^s \Delta x \end{array} \right] + Q_S \Delta x \Delta z = \left(S_1 + \Phi_f \right) \Delta x \Delta z \tag{A9}$$

where $Q_S = \bar{h}_{fF} \left(T_f - T_{F_i} \right) - \bar{h}_{Sf} \left(T_{S_o} - T_f \right)$ is the heat flux from the thin film into the shaft and into the top foil front surface. $\Phi_f = \dfrac{12 \mu_f}{h_f} \left\{ {W_f}^2 + \dfrac{1}{3} U_m + \left(U_f - U_m \right)^2 \right\}$ is the mechanical power converted into heat, and $S_1 = \left(U_f \, h_f \dfrac{\partial P_f}{\partial x} + W_f \, h_f \dfrac{\partial P_f}{\partial z} \right)$ is the (reversible) compression work.

Implementation of the upwind[6] scheme [13] for the thermal flux transport terms gives:

$$\left(\rho_f \, h_f \, U_f T_f \right)^e \Delta z = \dot{M}_e T_{f_e} = \left[\!\left[\dot{M}_e, 0 \right]\!\right] T_{f_P} - \left[\!\left[-\dot{M}_e, 0 \right]\!\right] T_{f_E}$$

[6] The numerical scheme follows prior work with bulk-flow models in high pressure annular seals.

$$\left(\rho_f\, h_f\, U_f T_f\right)^w \Delta z = \dot{M}_w T_{f_w} = \left[\!\left[\dot{M}_w, 0\right]\!\right] T_{f_W} - \left[\!\left[-\dot{M}_w, 0\right]\!\right] T_{f_P} \tag{A10}$$

$$\left(\rho_f\, h_f\, U_f T_f\right)^n \Delta x = \dot{M}_n T_{f_n} = \left[\!\left[\dot{M}_n, 0\right]\!\right] T_{f_P} - \left[\!\left[-\dot{M}_n, 0\right]\!\right] T_{f_N}$$

$$\left(\rho_f\, h_f\, U_f T_f\right)^s \Delta x = \dot{M}_s T_{f_s} = \left[\!\left[\dot{M}_s, 0\right]\!\right] T_{f_S} - \left[\!\left[-\dot{M}_s, 0\right]\!\right] T_{f_P}$$

where the mass flow rates are

$$\dot{M}_e = \left(\rho_f\, h_f\, U_f\right)^e \Delta z\,; \quad \dot{M}_w = \left(\rho_f\, h_f\, U_f\right)^w \Delta z\,; \tag{A11}$$

$$\dot{M}_n = \left(\rho_f\, h_f\, W_f\right)^n \Delta x\,; \quad \dot{M}_s = \left(\rho_f\, h_f\, W_f\right)^s \Delta x$$

i.e., identical to those in Eq. (A2). Above $\left[\!\left[A, B\right]\!\right]$ = max *(A,B)* . Substituting Eq. (A10) into Eq. (A9) and arranging leads to the algebraic equation for nodal temperatures:

$$A_{T_w} T_{f_W} + B_{T_p} T_{f_P} + C_{T_e} T_{f_E} + D_{T_N} T_{f_N} + D_{T_S} T_{f_S} = S_C^T \tag{A12}$$

where

$$A_{T_w} = c_{p_f} \left[\!\left[\dot{M}_w, 0\right]\!\right]; \quad C_{T_e} = c_{p_f} \left[\!\left[-\dot{M}_e, 0\right]\!\right];$$

$$D_{T_N} = c_{p_f} \left[\!\left[-\dot{M}_n, 0\right]\!\right]; \; D_{T_S} = c_{p_f} \left[\!\left[\dot{M}_s, 0\right]\!\right]$$

$$-B_{T_p} = C_{T_e} + A_{T_w} + D_{T_n} + D_{T_s} + S_P^T\,; \tag{A13}$$

and

$$S_P^T = \left(\overline{h}_{fF} + \overline{h}_{Sf}\right)\Delta x \Delta z\,; \quad S_C^T = -\left\{\left(\overline{h}_{fF} T_{F_i} + \overline{h}_{Sf} T_{S_o}\right) + S_1 + \Phi_f\right\}\Delta x \Delta z$$

The heat convection coefficients ($\overline{h}_{fF}$, $\overline{h}_{Sf}$) are derived using the Reynolds-Colburn analogy between fluid friction and heat transfer [20,21] for fully-developed flow, see Appendix B.

APPENDIX B: HEAT CONVECTION/CONDUCTION MODELS FOR GFBS

Heat transport from top foil into outer cooling stream and conduction into bearing housing

For a GFB and a hot hollow shaft, Figure B1 depicts the various heat flow paths and a simple representation with thermal resistances. The heat flow ($\dot{Q}_{f\to F}$) convected by the film into the top foil inner surface is conducted through the top foil and further conducted and advected into the bearing inner surface. The outer cooling gas stream flowing within the gap between the top foil and the bearing housing carries away heat ($\dot{Q}_{F\to O}$) conducted through the top foil backside, while the inner cooling gas stream flowing through the hollow shaft carries away heat ($\dot{Q}_{S\to C}$) convected from the hot shaft. The thin gas film also carries away heat ($\dot{Q}_{S\to f}$) from the hot shaft outer surface.

The radial heat flows through arc size $\Delta\Theta$, i.e. $\dot{Q} = \dot{q} R \Delta\Theta$. The heat flow rate $\dot{q}_{f\to F} = \bar{h}_{fF}\left(T_f - T_{F_i}\right)$ convected from the thin film into the top foil surface is further conducted through its thickness (Δ_{t_F}), and equals to

$$\dot{q}_{f\to F} = \frac{\kappa_F}{\Delta_{t_F}}\left(T_{F_i} - T_{F_o}\right) = \dot{q}_{F\to O} + \dot{q}_{F\to B_i} \qquad \text{(B1)}^7$$

where $\dot{q}_{F\to O} = \bar{h}_{FO}\left(T_{F_o} - T_O\right)$

is the heat convected into the outer cooling stream, and

$$\dot{q}_{F\to B_i} \approx \frac{\kappa_B}{\Delta_B}\left(T_{F_o} - T_{B_i}\right) \qquad \text{(B2)}$$

is the heat conducted through the material of the bump layer into the bearing housing.

[7] This equation is strictly valid for $R_{B_i} \approx R_{F_i} \approx R_{F_o}$

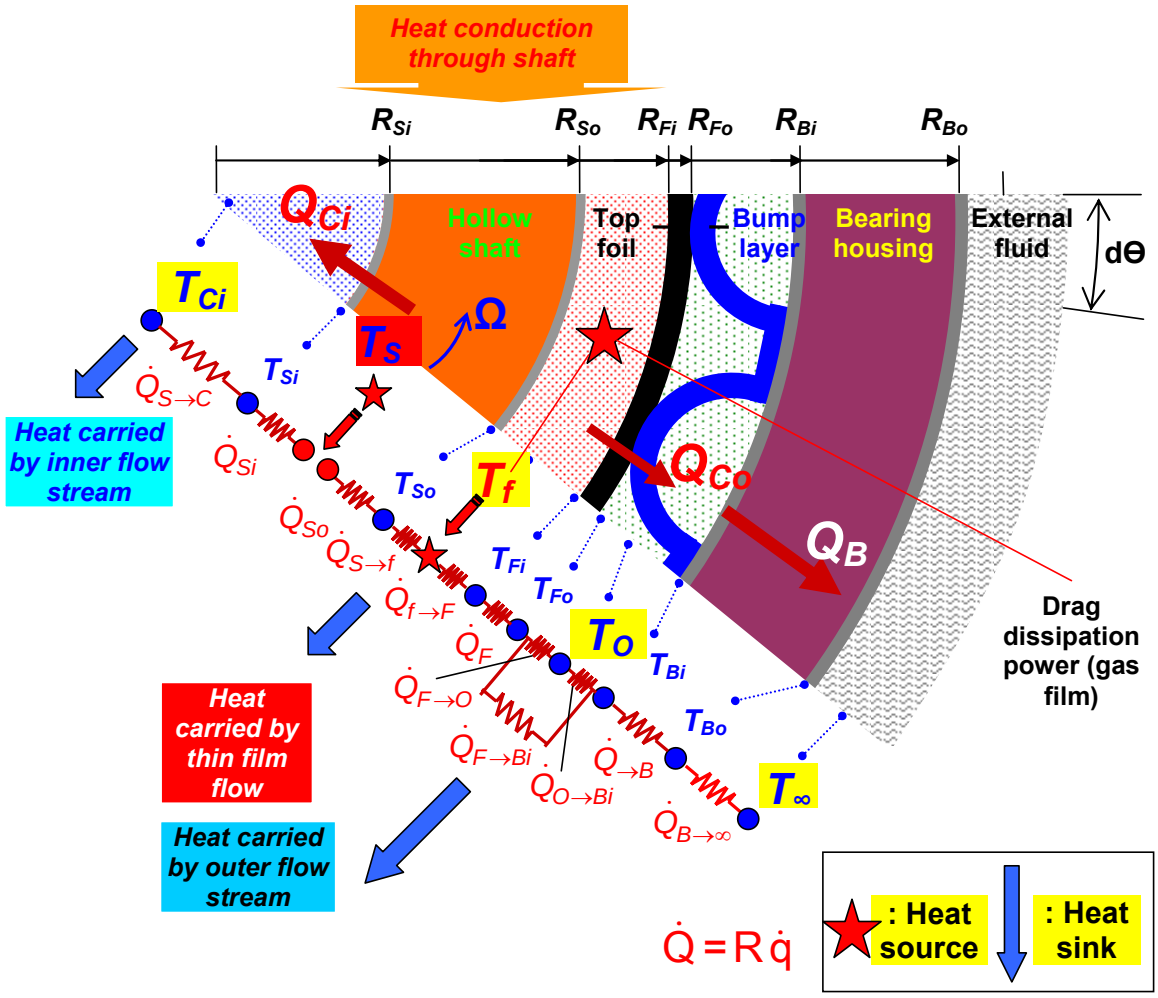

Figure B1. Simplified schematic diagram for heat flux paths in GFB system

The total heat flux into the bearing housing adds the convection from the outer flow stream and the conduction through the bump material, i.e.

$$\dot{q}_{\to B_i} = \dot{q}_{O\to B_i} + \dot{q}_{F\to B_i} = \bar{h}_{OB}\left(T_O - T_{B_i}\right) + \frac{\kappa_B}{\Delta_B}\left(T_{F_o} - T_{B_i}\right) \tag{B3}$$

For simplicity, assume only radial heat conduction through the bearing shell with thickness $\Delta_{t_B} = \left(R_{B_o} - R_{B_i}\right)$. Hence, a simple analysis shows that the heat flow rate per unit length equals

$$\left(\dot{q}_{\to B_i}\right) R_{B_i} = \dot{Q}_{\to B} = \frac{\kappa_B}{\ln\left(R_{B_o} \big/ R_{B_i}\right)}\left(T_{B_i} - T_{B_o}\right) \tag{B4}$$

where, for a thin bearing shell,

$$\dot{Q}_{\rightarrow B} \sim \frac{\kappa_B R_B}{\Delta_{t_B}} \left(T_{B_i} - T_{B_o} \right) \tag{B5}$$

Finally, the heat flux $\dot{Q}_{\rightarrow B}$ is disposed by convection into an external fluidic media at temperature T_∞.

$$\dot{Q}_{\rightarrow B} = \bar{h}_{B\infty} R_{B_o} \left(T_{B_o} - T_\infty \right) \tag{B6}$$

Above, $\bar{h}_{B\infty}$ is a heat convection coefficient depending on the external fluid material properties and flow conditions determining either natural or forced convection processes.

In spite of its apparent simplicity, the radial heat flow analysis will render foil ($\left(T_F\right)_{i,o}$ and bearing $\left(T_B\right)_{i,o}$ temperatures, as well as a cooling outer stream temperature (T_O) which vary in the circumferential and axial directions, i.e. $T_{B_i}\left(\Theta, z\right)$ for example.

Without an outer cooling flow stream, the heat transfer on the back of the top foil is by natural convection and further conduction into the bearing through the bump strip layers. In this **simplistic** scenario, the heat flow model is much simpler and fully described by an overall or equivalent heat transfer coefficient $\bar{h}_{eq}$ that represents a multilayer conduction/convection. The heat flow convected by the film into the top foil inner surface is conducted through the top foil and further conducted and advected into the bearing inner surface, i.e.

$$\dot{Q}_{f\rightarrow F} = \bar{h}_{fF} R_{F_i} \left(T_f - T_{F_i} \right)$$

$$\rightarrow = \dot{Q}_{\rightarrow F} = \frac{\kappa_F R_F}{\Delta_{t_F}} \left(T_{F_i} - T_{F_o} \right) \tag{B7}$$

$$\rightarrow = \dot{Q}_{F\rightarrow B} = \bar{h}_{FO} R_{F_o} \left(T_{F_o} - T_O \right) + \frac{\kappa_F}{\Delta_B} R_{B_{eq}} \left(T_{F_o} - T_{B_i} \right)$$

where a bump *equivalent* radius $R_{B_{eq}} = \frac{\Delta_{t_B} N_B}{\pi}$ denotes the narrow contact area (/axial length) of N_B bumps with thickness Δ_{t_B}.

Since the outer stream is stagnant, then,

$$\dot{Q}_{F\to O} = \bar{h}_{FO}\, R_{F_o}\left(T_{F_o} - T_O\right) \to = \dot{Q}_{O\to B_i} = \bar{h}_{OB}\, R_{B_i}\left(T_O - T_{Bi}\right) .$$

In the absence of an outer cooling stream, the heat flow is conducted into the bearing to be finally disposed into an external fluidic medium at T_∞, i.e.

$$\dot{Q}_{F\to B} \to = \dot{Q}_{\to B} = \frac{\kappa_B}{\ln\left(R_{B_o} \big/ R_{B_i}\right)}\left(T_{B_i} - T_{B_o}\right) \tag{B8}$$

$$\to = \dot{Q}_{B\to\infty} = \bar{h}_{B\infty}\, R_{B_o}\left(T_{B_o} - T_\infty\right)$$

Eliminate the internal temperatures in the equations above by adding each heat flow divided by its respective thermal conductance (=1/resistance). This simple process leads to

$$\dot{Q}_{f\to F} = \dot{q}_{f\to F} R_{F_i} = \bar{h}_{eq_\infty}\, R_{F_i}\left(T_f - T_\infty\right) \tag{B8}$$

where the equivalent heat transfer coefficient is

$$\frac{1}{\bar{h}_{eq_\infty}} = \frac{1}{\bar{h}_{fF}} + \frac{1}{\dfrac{\kappa_F}{\Delta_{t_F}}} + \frac{R_{F_i}}{R_{B_{eq}}\dfrac{\kappa_F}{\Delta_B} + \dfrac{1}{\dfrac{1}{R_{F_o}\bar{h}_{FO}} + \dfrac{1}{R_{B_i}\bar{h}_{OB}}}} + \frac{R_{F_i}\ln\left(\dfrac{R_{Bo}}{R_{Bi}}\right)}{\kappa_B} + \frac{R_{F_i}}{h_{B\infty}R_{Bo}} \tag{B9}$$

Conversely, **an outer cooling stream with a large flow rate** takes away most of the heat from the back of the top foil, with little conduction into the bearing. In this case, the heat flow reduces to the simple expression

$$\dot{Q}_{f\to F} = \dot{q}_{f\to F} R_{F_i} = \bar{h}_{eq_O}\, R_{F_i}\left(T_f - T_O\right) \tag{B10}$$

$$\frac{1}{\bar{h}_{eq_O}} = \frac{1}{\bar{h}_{fF}} + \frac{\Delta_{t_F}}{\kappa_F} + \frac{R_{F_i}}{R_{F_o}\bar{h}_{FO}} \tag{B11}$$

as also given by Peng and Khonsari [7].

Temperature field in rotating shaft

The inner cooling gas stream flowing through the hollow shaft is regarded as a sink of thermal energy. That is, this cooling mass flow rate is large enough to maintain a constant temperature T_{C_i} while advecting (removing) heat flow from the shaft inner surface [8] at temperature T_{S_i}. Note that the thin gas film with temperature T_f also carries away heat from the shaft outer surface at temperature T_{S_o}.

The energy transport equation for the rotating shaft in polar coordinates ($r,\Theta.z$) is [22]

$$c_{P_S}\rho_S\,\Omega\frac{\partial T_S}{\partial\Theta}=-\left[\frac{1}{r}\frac{d}{dr}\left(r\,\dot{q}_{r_S}\right)+\frac{1}{r}\frac{d}{d\Theta}\left(\dot{q}_{\Theta_S}\right)+\frac{d}{dz}\left(\dot{q}_{z_S}\right)\right] \tag{B12}$$

where the components of the heat flux vector are

$$\dot{q}_{\Theta_S}=-\kappa_S\frac{1}{r}\frac{\partial T_S}{\partial\Theta};\ \dot{q}_{r_S}=-\kappa_S\frac{\partial T_S}{\partial r};\ \dot{q}_{z_S}=-\kappa_S\frac{\partial T_S}{\partial z}; \tag{B13}$$

The shaft temperature must be periodic in the circumferential direction. Hence, $T_S\left(\Theta,r,z\right)=T_S\left(\Theta+2\pi,r,z\right)$. Other **boundary conditions** include

a) Heat convection through inner and outer surfaces of hollow shaft, i.e.

$$\text{At}\quad r=R_{S_i}\qquad\left[-\dot{q}_{r_{S_i}}\,R_{S_i}\right]=\dot{Q}_{S\to C_i}=R_{S_i}\,\bar{h}_{SC_i}\left(T_{S_i}-T_{C_i}\right) \tag{B13}$$

$$\text{And,}\ r=R_{S_o}\qquad\left[\dot{q}_{r_{S_o}}\,R_{S_o}\right]=\dot{Q}_{S\to f}=R_{S_o}\,\bar{h}_{Sf}\left(T_{S_o}-T_f\right); \tag{B14}$$

Recall $\dot{Q}_{S\to f}=\dot{q}_{S\to f}\,R_{S_o}$. The equations above show the heat flows removed by the inner cooling stream and by the thin gas film, respectively.

b) Specification of shaft temperature at $z=0$ and $z=L$ for $\left\{0\le\Theta\le2\pi;R_{S_i}\le r\le R_{S_o}\right\}$. Accurate (a-priori) knowledge of the shaft temperature fields at the inlet and exit axial planes is quite difficult. In actuality, the model should not just consider a piece of hollow shaft of length L but rather a longer shaft span with physically known operating temperature conditions.

Presently, assume for simplicity:

1. The inner cooling stream flow is so large that the shaft inner surface temperature T_{S_i} does not vary axially or circumferentially, i.e. it is a constant; and

[8] Recall that the shaft is regarded as *hot* with temperature $T_S > T_f > T_C$.

2. A high speed (Ω) rotor condition tends to make more uniform the shaft temperature in the circumferential direction.

The considerations above imply that most of the heat flow within the shaft is transported radially. Hence, $\dot{q}_{\Theta_S} = \dot{q}_{z_S} = 0$; $\dot{q}_{r_S} = -\kappa_S \dfrac{d T_S}{d r}$; and the heat conduction Eq. (B12) reduces to

$$\frac{1}{r}\frac{d}{d r}\left(r\,\dot{q}_{r_S}\right) = 0 \rightarrow \frac{1}{r}\frac{d}{d r}\left(r\frac{d T_S}{d r}\right) = 0 \tag{B15}$$

Integration of this equation leads to a shaft temperature distribution along the radial coordinate equal to

$$T_S(r) = T_{S_i} + \left(T_{S_o} - T_{S_i}\right)\frac{\ln\left(r \big/ R_{S_i}\right)}{\ln\left(R_{S_o} \big/ R_{S_i}\right)} \tag{B13}$$

And from the heat convection at the inner and outer surfaces of the hollow shaft,

$$-\dot{Q}_{S\rightarrow C_i} = -R_{S_i}\,\overline{h}_{SC_i}\left(T_{S_i} - T_{C_i}\right) = \dot{Q}_{S\rightarrow f} = R_{S_o}\,\overline{h}_{Sf}\left(T_{S_o} - T_f\right) \tag{B14}$$

The equation above is incompatible with the assumption of pure radial heat flow and a *hot shaft* since it requires that if $\left(T_{S_i} - T_{C_i}\right) > 0 \rightarrow \left(T_f - T_{S_o}\right) > 0$, i.e. heat flows from the thin film into the shaft. More scrutiny of the heat conduction model is thus needed.

However, if the whole shaft is regarded at a uniform *hot* temperature, then $T_{S_i} = T_{S_o} = T_S$, and heat can flow into the thin film and/or into the cooling stream. Note that in this case, the shaft acts as a source of thermal energy with heat flowing along two opposite radial directions, i.e. through the inner and outer surfaces of the hollow shaft.

Table B1 summarizes each of the heat flows and their relevant physical description. See Fig. B1 for a definition of all temperatures, interfacial and within solids.

Table B1 Summary of radial heat flows (convection and conduction)

Heat flow per unit axial length	Description
$\dot{Q}_{f\to F} = \dot{q}_{f\to F}\, R_{F_i} = \bar{h}_{fF}\, R_{F_i}\left(T_f - T_{F_i}\right)$	Heat convected from thin film into front (inner) surface of top foil
$\dot{Q}_{\to F} = \dfrac{\kappa_F\, R_F}{\Delta_{t_F}}\left(T_{F_i} - T_{F_o}\right)$	Heat conducted through top foil (inner to outer surfaces)
$\dot{Q}_{F\to B} = \dfrac{\kappa_F}{\Delta_B}\, R_{B_{eq}}\left(T_{F_o} - T_{B_i}\right)$	Heat conducted through bump foil – from top foil back surface into bearing inner surface
$\dot{Q}_{F\to O} = \bar{h}_{FO}\, R_{F_o}\left(T_{F_o} - T_O\right)$	Heat convected from back surface of top foil into cooling outer stream
$\dot{Q}_{O\to B_i} = \bar{h}_{OB}\, R_{B_i}\left(T_O - T_{B_i}\right)$	Heat convected from cooling outer stream into bearing inner surface
$\dot{Q}_{\to B} = \dfrac{\kappa_B}{\ln\left(R_{B_o} \big/ R_{B_i}\right)}\left(T_{B_i} - T_{B_o}\right)$	Heat conducted through bearing shell
$\dot{Q}_{B\to\infty} = \bar{h}_{B\infty}\, R_{B_o}\left(T_{B_o} - T_\infty\right)$	Heat convected from outer surface of bearing into external fluid medium
$\dot{Q}_{S\to f} = \dot{q}_{S\to f}\, R_{S_o} = \bar{h}_{Sf}\, R_{S_o}\left(T_{S_o} - T_f\right)$	Heat convected from shaft outer surface into gas film
$\dot{Q}_{\to S} = \dfrac{\kappa_S\left(T_{S_i} - T_{S_o}\right)}{\ln\left(\dfrac{R_{S_i}}{R_{S_o}}\right)}$	Heat conducted through hollow shaft
$-\dot{Q}_{S\to C_i} = \bar{h}_{SC_i}\, R_{S_i}\left(T_{S_i} - T_{C_i}\right)$	Heat from hollow shaft convected by cooling inner stream

Heat transfer convection coefficients **(Taken from [21])**

The Reynolds-Colburn analogy between fluid friction and heat transfer [20,21] for fully-developed flow is used to determine the heat convection coefficients. The mean heat transfer over the entire laminar/turbulent boundary is:

$$S_t\, \wp_r^{2/3} = f/2 \qquad \text{(B15)}$$

where $S_t = \dfrac{\bar{h}_t}{\rho c_p V_t}$ is the *Stanton* number, and $\wp_r = \dfrac{c_p \mu}{\kappa}$ is the *Prandtl* number, and

$f = a_m \left[1 + \left(c_m \dfrac{r}{H} + \dfrac{b_m}{R_e} \right)^{e_m} \right]$ is the *Fanning* friction factor based on *Moody's equation*. Above V_t is a characteristic fluid velocity relative to the velocity of the surface of interest. From the relationships above, the heat convection coefficient is:

$$\bar{h}_t = \frac{1}{2} \frac{\rho c_p V_t f}{\wp_r^{2/3}} \tag{B16}$$

and by analogy, $$\bar{h}_B = \frac{1}{2} \frac{\rho c_p V_B f_B}{\wp_r^{2/3}}; \quad \bar{h}_J = \frac{1}{2} \frac{\rho c_p V_J f_J}{\wp_r^{2/3}} \tag{B17}$$

Where $V_{B,J}$ and $f_{B,J}$ are the fluid velocities and friction factors relative to the bearing and journal surfaces.

In a centered journal bearing with characteristic clearance c, the mean velocities $V_{B,J} \sim \frac{1}{2}\, \Omega R$. The friction factor for laminar flow is $f = 12/\mathrm{Re}_c$, where $\mathrm{Re}_c = \dfrac{\rho \Omega R c}{\mu}$ is the circumferential flow Reynolds number. Algebraic substitution of f into Eqs. (B17) renders

$$\bar{h}_B = \bar{h}_J = 3 \frac{\kappa}{c} \wp_r^{1/3} \big|_{\text{laminar flow}} \text{ or } Nu = \frac{c \bar{h}}{\kappa} = 3\, \wp_r^{1/3} \tag{B18}$$

The archival literature presents many other formulas – empirically based - for turbulent flow heat transfer coefficients, including evolving or fully developed thermal conditions, as well as for fixed wall temperature or constant heat flux into a wall. For example, a well known formula for turbulent flow conditions sets the Nusselt number as [21]

$$Nu = \frac{c_* \bar{h}}{\kappa} = 0.023\, \mathrm{Re}^{0.8}\, \wp_r^{1/3} \tag{B19}$$

where $c_* = \Delta_B$ is a characteristic length for the outer cooling stream, and Re is an axial flow Reynolds number, a function of the axial pressure drop $\left(P_{C_i} - P_a \right)$.

APPENDIX C: AIR PROPERTIES AS A FUNCTION OF TEMPERATURE

Figures C1 and C2 depict the air material properties μ and κ versus temperature, as implemented in the analysis program. The graphs include predictive formulas, and where (x) and (y) denote the variables in the horizontal and vertical axes, respectively. The linear fit correlation coefficients (R^2) are close to unity. Note that gas specific heat (c_p) is taken as a constant (1,020 J/kg K) since it does not change significantly with temperature. For example, c_p varies from 1,005 J/kg K at -150 °C to 1,067 J/kg K at 400 °C [17].

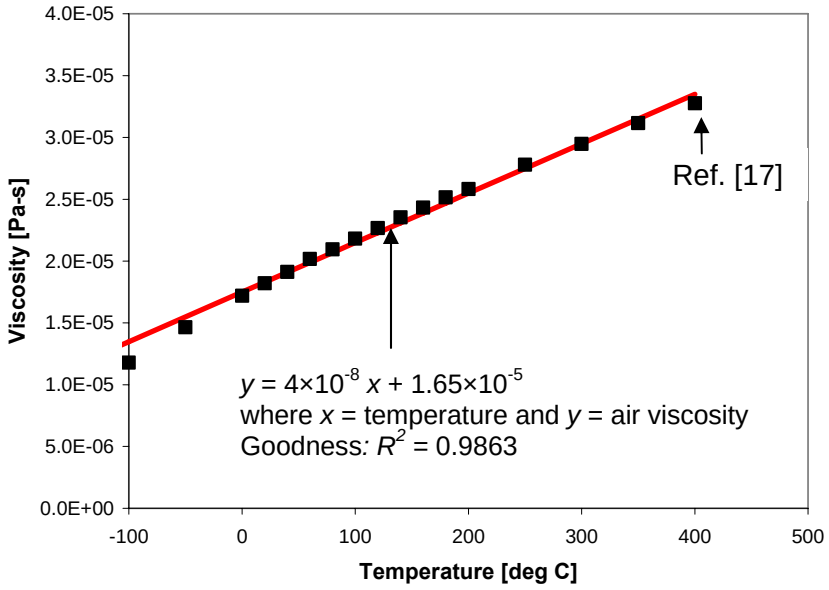

Figure C1. Air viscosity versus temperature [17]

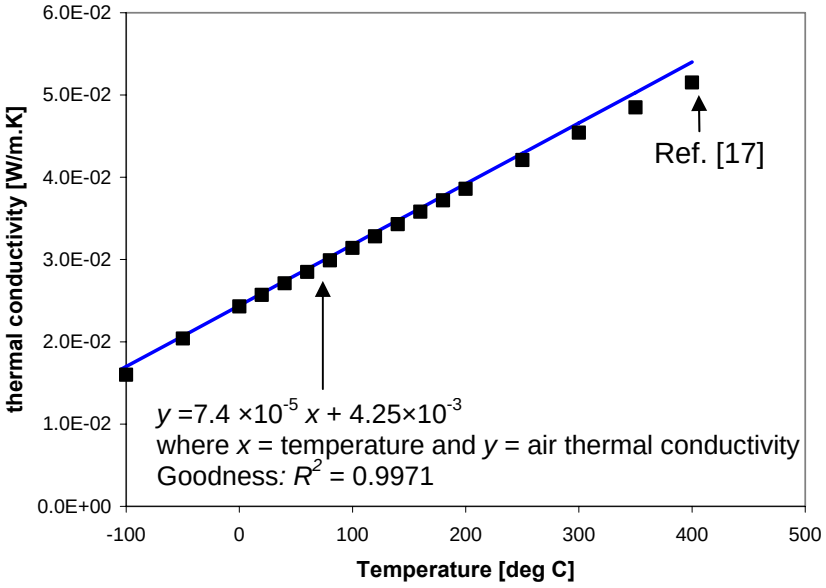

Figure C1. Air thermal conductivity versus temperature [17]

APPENDIX D: CENTRIFUGAL GROWTH AND THERMAL EXPANSIONS OF SHAFT AND BEARING CARTRIDGE

Centrifugal growth (S_C) of the rotating shaft reduces the actual bearing clearance as the rotor speed (Ω) increases. The shaft growth depends on the shaft geometry and material properties [23]:

$$S_C = \frac{R_o \rho_s \Omega^2}{8E_S}\left\{(1-\nu_s)A_1 + (1-\nu_s)A_2 - (1-\nu_s^2)R_o^2\right\} \quad \text{(C1)}$$

$$A_1 = \left(R_o^2 + R_i^2\right)(3+\nu_s) \qquad A_2 = R_i^2(3+\nu_s)$$

where E_s, ν_s, and ρ_s are the shaft elastic modulus, Poisson ratio, and density, respectively. The shaft has an outer radius R_o and, if hollow, an inner radius R_i. Figure D1 shows the calculated shaft centrifugal growth versus rotor speed for an alloy steel (AISI 4140 [24]) solid shaft (R_o = 19.05 mm, R_i =0 mm) and hollow shafts with (R_i = 12.7mm$_o$ and R_i = 6.4 mm). The shaft centrifugal growth increases dramatically as the rotating speed increase, i.e., $S_C \sim \Omega^2$, in particular for a hollow shaft with a large inner diameter, i.e. a thin wall. At a high rotating speed of 100 krpm, a hollow shaft with (R_i = 12.7mm$_o$) has a radial growth of 17 μm, i.e., ~24 % of the nominal radial clearance of 70 μm, for example.

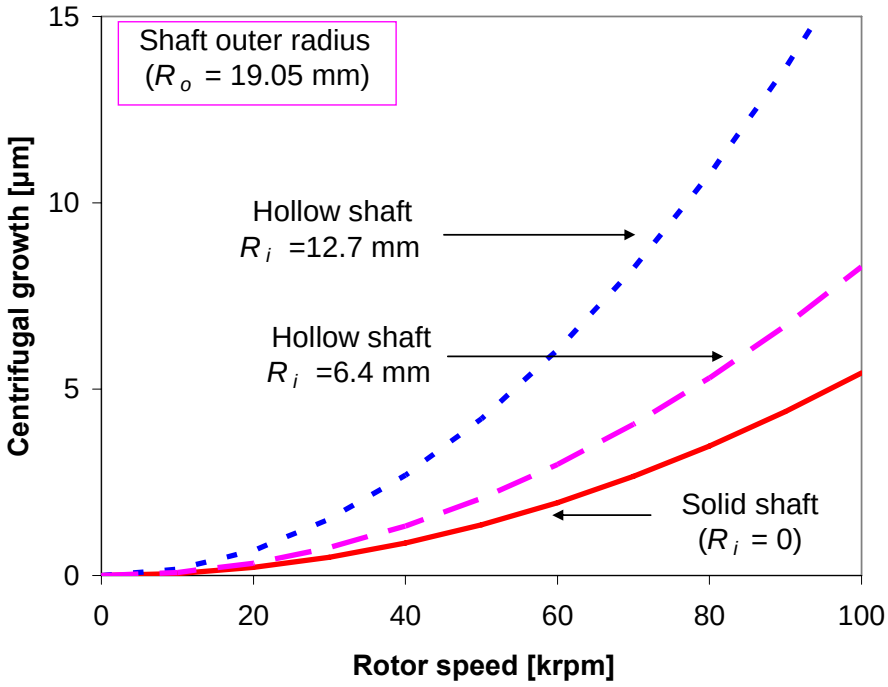

Figure D1. Centrifugal shaft growth versus increasing rotor speed for an alloy steel (AISI 4140) shaft with an outer radius R_o = 19.05 mm. Solid shaft (R_i=0) and hollow shafts with inner radii (R_i=6.4 mm, and R_i=12.7 mm)

Shaft (or bearing) thermal expansion (S_T) is proportional to the temperature difference (ΔT) through the material thermal expansion coefficient (α_T) [25], i.e.

$$S_T = \alpha_T R_o \Delta T \tag{C2}$$

As the rotor speed and static load increase, an increase in the thin film temperature causes thermal expansion of the rotating shaft and the bearing housing. For typical shaft and bearing materials (Inconel 718, Inconel X750, AISI 304, and AISI 4140 Steel) with a radius of 19.05 mm, Fig. D2 shows shaft thermal expansion versus temperature. The thermal expansion coefficients for Inconel 718, Inconel X750, AISI 304, and AISI 4140 steel are 13 $\times 10^{-6}$ 1/K, 12 $\times 10^{-6}$ 1/K, 18 $\times 10^{-6}$ 1/K, and 12.3 $\times 10^{-6}$ 1/K respectively [24, 26-28]. For the AISI 4140 steel with a thermal expansion coefficient α_T = 12.3 $\times 10^{-6}$ 1/K, the thermal expansion is as large as 32 µm, almost half the FB nominal radial clearance of 70 µm, at a moderately high temperature of 150 °C. The findings above thus reveal the need for an adequate cooling mechanism (proven thermal management) in high temperature GFBs.

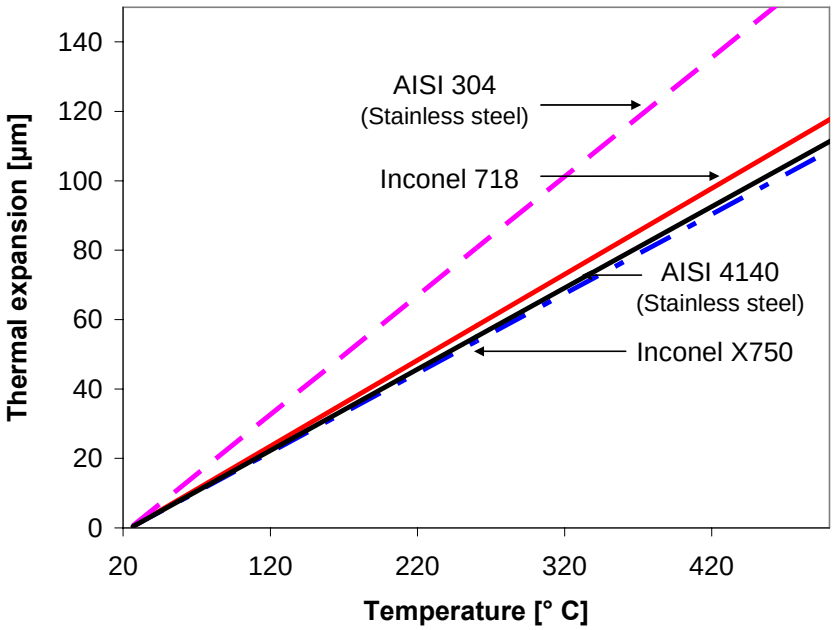

Figure D2. Shaft thermal expansion versus temperature for typical shaft and bearing materials

APPENDIX E: FOIL MATERIAL PROPERTIES FOR INCREASING TEMPERATURES

The predictions also account for the effect of temperature on the mechanical properties of the bump foil structure. Accurate prediction of GFB performance at high temperatures requires incorporating changes in the structural stiffness and thermal conductivity of the underlying foil structure. Inaccurate thermal models without considerations of the heat flux into the bearing structure can easily lead to incorrect predictions.

Figure E1 shows the modulus of elasticity versus temperature for Inconel X750 super alloy, a typical foil material. As the temperature increases from 20 °C to 800 °C the modulus of elasticity decreases from 214 GPa to 120 GPa (40 % decrease). In actual GFB operation, the large variation of the modulus of elasticity will change a bump foil stiffness. Thermal conductivity of the Inconel X750 foil material, which increases with temperature, as shown in Fig. E2 can also affect the force coefficients of GFBs.

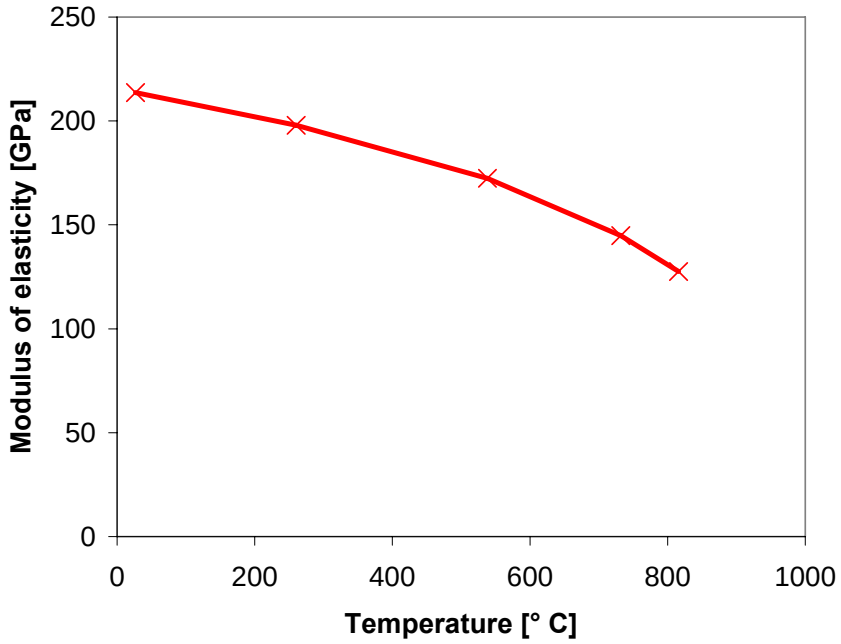

Figure E1. Modulus of elasticity versus temperature for Inconel X750 super alloy [27]

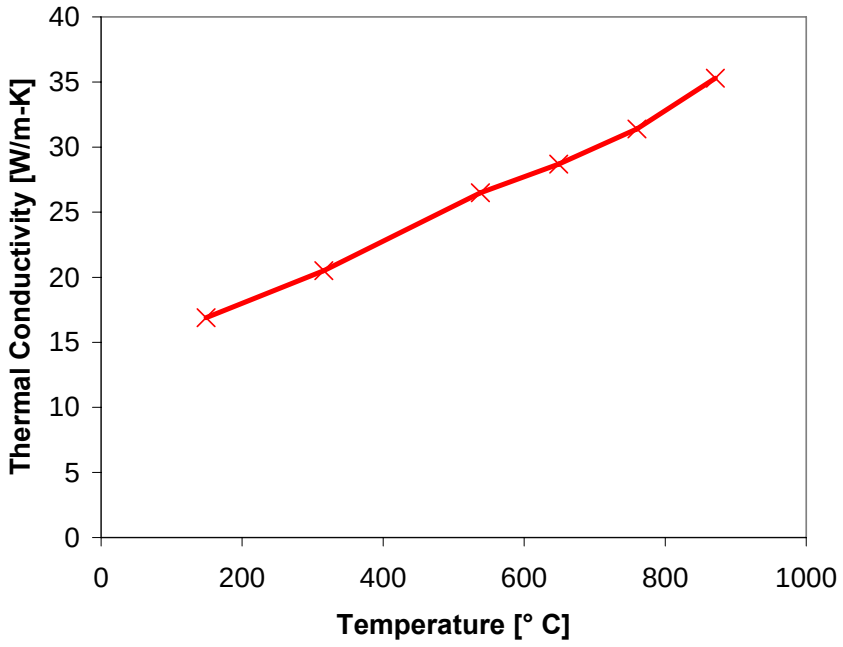

Figure E2. Thermal conductivity versus temperature for Inconel X750 super alloy [27]